

## Lyman Continuum Emission from AGN at $2.3 \lesssim z \lesssim 3.7$ in the UVCANDELS Fields

BRENT M. SMITH,<sup>1</sup> ROGIER A. WINDHORST,<sup>1</sup> HARRY TEPLITZ,<sup>2</sup> MATTHEW HAYES,<sup>3</sup> MARC RAFELSKI,<sup>4,5</sup> MARK DICKINSON,<sup>6</sup> VIHANG MEHTA,<sup>7</sup> NIMISH P. HATHI,<sup>4</sup> JOHN MACKENTY,<sup>4</sup> L. Y. AARON YUNG,<sup>8</sup> ANTON M. KOEKEMOER,<sup>4</sup> EMMARIS SOTO,<sup>9</sup> CHRISTOPHER J. CONSELICE,<sup>10</sup> RAY A. LUCAS,<sup>4</sup> XIN WANG,<sup>11,12,13</sup> KEUNHO J. KIM,<sup>14</sup> ANAHITA ALAVI,<sup>7</sup> NORMAN A. GROGIN,<sup>4</sup> BEN SUNNQUIST,<sup>4</sup> LAURA PRICHARD,<sup>4</sup> ROLF A. JANSEN,<sup>1</sup> AND THE UVCANDELS TEAM

<sup>1</sup>School of Earth & Space Exploration, Arizona State University, Tempe, AZ 85287-1404, USA

<sup>2</sup>Euclid NASA Science Center at IPAC, California Institute of Technology, Pasadena, CA 91125, USA

<sup>3</sup>Stockholm University, Department of Astronomy and Oskar Klein Centre for Cosmoparticle Physics, AlbaNova University Centre, SE-10691, Stockholm, Sweden

<sup>4</sup>Space Telescope Science Institute, Baltimore, MD 21218, USA

<sup>5</sup>Department of Physics and Astronomy, Johns Hopkins University, Baltimore, MD 21218, USA

<sup>6</sup>NSF's NOIRLab, Tucson, AZ 85719, USA

<sup>7</sup>IPAC, Mail Code 314-6, California Institute of Technology, 1200 E. California Blvd., Pasadena CA, 91125, USA

<sup>8</sup>Astrophysics Science Division, NASA Goddard Space Flight Center, Greenbelt, MD 20771, USA

<sup>9</sup>Computational Physics, Inc., Springfield, VA 22151, USA

<sup>10</sup>Jodrell Bank Centre for Astrophysics, University of Manchester, Oxford Road, Manchester M13 9PL, UK

<sup>11</sup>School of Astronomy and Space Science, University of Chinese Academy of Sciences (UCAS), Beijing 100049, China

<sup>12</sup>Institute for Frontiers in Astronomy and Astrophysics, Beijing Normal University, Beijing 102206, China

<sup>13</sup>National Astronomical Observatories, Chinese Academy of Sciences, Beijing 100101, China

<sup>14</sup>IPAC, California Institute of Technology, Pasadena, CA 91125, USA

### Abstract

We present the results of our search for Lyman continuum (LyC) emitting (weak) AGN at redshifts  $2.3 \lesssim z \lesssim 4.9$  from Hubble Space Telescope (HST) Wide Field Camera 3 (WFC3) F275W observations in the UVCANDELS fields. We also include LyC emission from AGN using HST WFC3 F225W, F275W, and F336W found in the ERS and HDUV data. We performed exhaustive queries of the Vizier database to locate AGN with high quality spectroscopic redshifts. In total, we found 51 AGN that met our criteria within the UVCANDELS and ERS footprints. Out of these 51, we find 12 AGN had  $\geq 4\sigma$  detected LyC flux in the WFC3/UVIS images. Using a wide variety of space-based plus ground-based data, ranging from X-ray to radio wavelengths, we fit the multi-wavelength photometric data of each AGN to a CIGALE SED using AGN models and correlate various SED parameters to the LyC flux. KS-tests of the SED parameter distributions for the LyC-detected and non-detected AGN showed they are likely not distinct samples. However, we find that X-ray luminosity, star-formation onset age, and disk luminosity show strong correlations relative to their emitted LyC flux. We also find strong correlation of the LyC flux to several dust parameters, i.e., polar and toroidal dust emission,  $6\mu\text{m}$  luminosity, and anti-correlation with metallicity and  $A_{\text{FUV}}$ . We simulate the LyC escape fraction ( $f_{\text{esc}}$ ) using the CIGALE and IGM transmission models for the LyC-detected AGN and find an average  $f_{\text{esc}} \simeq 18\%$ , weighted by uncertainties. We stack the LyC flux of subsamples of AGN according to the wavelength continuum region in which they are detected and find no significant distinctions in their LyC emission, although our *sub-mm* detected F336W sample ( $3.15 < z < 3.71$ ) shows the brightest stacked LyC flux. These findings indicate that LyC-production and -escape in AGN is more complicated than the simple assumption of thermal emission and a 100% escape fraction. Further testing of AGN models with larger samples than presented here is needed.

### 1. INTRODUCTION

The end of the Reionization epoch has been constrained to  $z \sim 6$  by multiple studies of Gunn-Peterson troughs seen in AGN spectra (e.g., Becker et al. 2001; Djorgovski et al. 2001; Fan et al. 2006; Goto et al. 2011), though more re-

cent evidence has been presented favoring a longer epoch ending around  $z \sim 5.3\text{--}5.5$  (e.g., Qin et al. 2021; Bosman et al. 2022; Zhu et al. 2023). The leading candidates for the main producers of Hydrogen ionizing radiation ( $\lambda \leq 912\text{\AA}$ , i.e., Lyman Continuum (LyC)) are thought to be low-mass, star-forming galaxies which existed in abundance at  $z \gtrsim 6$  (e.g., Bouwens et al. 2015; Parsa et al. 2018; Saldana-Lopez et al. 2023). However, direct observation of their LyC escape fraction ( $f_{\text{esc}}$ ) is impossible due to the IGM opacity, and investigations into low- $z$  analogues show the  $f_{\text{esc}}$  is low (e.g.,

Corresponding author: Brent M. Smith  
 bsmith18@asu.edu

Rutkowski et al. 2017; Marchi et al. 2018; Steidel et al. 2018; Pahl et al. 2021; Griffiths et al. 2022, but see, e.g., Leitherer et al. 2016; Izotov et al. 2021; Flury et al. 2022 for local LyC emitting analogues). Furthermore, there is evidence for older stellar populations existing before Reionization completed (e.g., Hashimoto et al. 2018; Laporte et al. 2021; Tacchella et al. 2023), indicating that Reionization completion lagged behind significant star formation during galaxy assembly.

In order to be compatible with the observed rapid Reionization scenario of  $\lesssim 100$  Myr (Bolan et al. 2022), a second population of low mass, star forming galaxies with high LyC escape must have formed ubiquitously in the Universe from  $6 \lesssim z \lesssim 8$ . These galaxies would require a stellar IMF such that enough supernovae could clear out neutral hydrogen in the ISM via outflows and winds to allow high mass, main sequence stars to emit the sufficient amount of LyC to reionize the IGM with  $f_{\text{esc}} \simeq 10\text{--}20\%$  (Finkelstein et al. 2019; Yung et al. 2020b,a; Mutch et al. 2023). These conditions may be able to be met given the rising star-formation histories in some bright  $z > 7$  galaxies observed with JWST (e.g., Finkelstein et al. 2022; Giménez-Arteaga et al. 2023; Robertson et al. 2023; Tacchella et al. 2023). Alternatively, a significant population of low luminosity AGN at  $z > 6$  could contribute substantially to the completion of hydrogen Reionization (Giallongo et al. 2015; Madau & Haardt 2015; Khaire et al. 2016; Grazian et al. 2018, 2020; Yung et al. 2021; Grazian et al. 2022; Onoue et al. 2023). This AGN Reionization paradigm is reinforced by the discovery of  $10^8\text{--}10^9 M_{\odot}$  quasars at  $z > 7$  when the universe was  $\sim 750$  Myr old (Mortlock et al. 2011; Bañados et al. 2018; Wang et al. 2018; Matsumura et al. 2019; Yang et al. 2019, 2020; Wang et al. 2021), which indicates high efficiency accretion onto super massive black holes (SMBHs) while the IGM was being reionized. Furthermore, recent studies of the  $z \gtrsim 5$  AGN luminosity function and space density suggest that faint ( $M_{1450} \simeq -23$ ) AGN are  $\sim 3\text{--}5$  times more abundant at  $z \sim 5$  than previous work (e.g., McGreer et al. 2018; Niida et al. 2020; Kim et al. 2020), and a slower evolution of the space density from  $3 \lesssim z \lesssim 6$  is observed (e.g., Giallongo et al. 2019; Grazian et al. 2022; Fontanot et al. 2023).

It is most likely the case that stars in massive and low-mass galaxies, as well as AGN, contributed to Reionization. The timeline for which sources dominated the ionizing background, and the characteristics of sources with high  $f_{\text{esc}}$  remain unclear. In this work, we focus on characterizing the physical properties of AGN with high and low LyC emission using imaging from the HST UVCANDELS program (Wang et al. 2023), which expands on our work from Smith et al. (2018, 2020) using WFC3/UVIS ERS (Windhorst et al. 2011) and HDUV (Oesch et al. 2018) imaging. These constraints can be extrapolated to AGN found during the Reionization epoch, and provide further insight into the role of AGN as reionizers of the IGM, since AGN SED shapes are known to not evolve with cosmic time (e.g., Shen et al. 2019; Yang et al. 2021). We present our analysis as follows: in §2 we describe the data we use for LyC measurement; in §3 we detail our sample selection of AGN used for our LyC stud-

ies; in §4 we review our CIGALE SED fitting configuration and the ancillary photometry used for fitting; in §5 we outline our LyC photometry and  $f_{\text{esc}}$  methodology; in §6 we present our results; in §7 we discuss our results, and in §8 we summarize our conclusions. We assume [Planck Collaboration \(2020\)](#) cosmology (flat  $\Lambda$ CDM,  $H_0 = 67.4 \text{ km s}^{-1} \text{ Mpc}^{-1}$ ,  $\Omega_m = 0.315$ ) and use AB magnitudes (Oke & Gunn 1983) throughout.

## 2. DATA

Our main image data used for studying the LyC emission from AGN was collected as part of the Ultraviolet Imaging of the Cosmic Assembly Near-infrared Deep Extragalactic Legacy Survey Fields (UVCANDELS) program (Teplitz 2018). This UV imaging covers the COSMOS, EGS, and completes the GOODS North and South fields in F275W with a 3-orbit depth and coordinated parallels using the F435W filter with the Advanced Camera for Survey (ACS). The F435W exposures have some variation in depth due to roll angle constraints and overlap with other exposures. This data can be found on MAST via [10.17909/fw24-0b81](#). UVCANDELS also includes ground-based Large Binocular Telescope U-band imaging in GOODS North and COSMOS that probes down to  $m_{AB} \sim 28$  mag (Ashcraft et al. 2018, 2023; Otteson et al. 2021; Redshaw et al. 2022). We also include UV imaging from the Hubble Deep UV Legacy survey (HDUV; Oesch et al. 2018), the Hubble Ultraviolet Ultra Deep Field (UVUDF; Teplitz et al. 2013; Rafelski et al. 2015), and Early Release Science field (ERS; Windhorst et al. 2011) in F225W, F275W, and F336W for our AGN LyC analysis when available. The various depths reached by each survey are captured in the photometric uncertainties (see §4.1). Further details on the image quality and drizzling parameters of the UVCANDELS imaging can be found in Wang et al. (2023).

## 3. SAMPLE SELECTION

Our spectroscopically verified AGN sample was initially compiled from queries of the Vizier database (Ochsenbein et al. 2000) for AGN catalogs and the NASA/IPAC Extragalactic Database (NED)<sup>1</sup> for QSOs. LyC from AGN can be safely observed with negligible non-ionizing contamination at redshifts  $2.26 \leq z < 2.47$ ,  $2.47 \leq z < 3.08$ , and  $z \geq 3.08$  in WFC3/UVIS F225W, F275W, and F336W images, respectively (Smith et al. 2018). We therefore selected catalogs and NED objects with spectroscopic redshifts from  $2.26 \leq z < 5$ , and extracted AGN from the selected catalogs (Véron-Cetty & Véron 2006; Donley et al. 2007; Cardamone et al. 2008; Souchay et al. 2012; Kirkpatrick et al. 2012; Gattano et al. 2014; Brightman et al. 2014; Souchay et al. 2015; Rosen et al. 2016; Xue et al. 2016; Del Moro et al. 2016; Tie et al. 2017; Luo et al. 2017; Guidetti et al. 2017; Liu et al. 2018)

<sup>1</sup> The NASA/IPAC Extragalactic Database (NED) is funded by the National Aeronautics and Space Administration and operated by the California Institute of Technology.

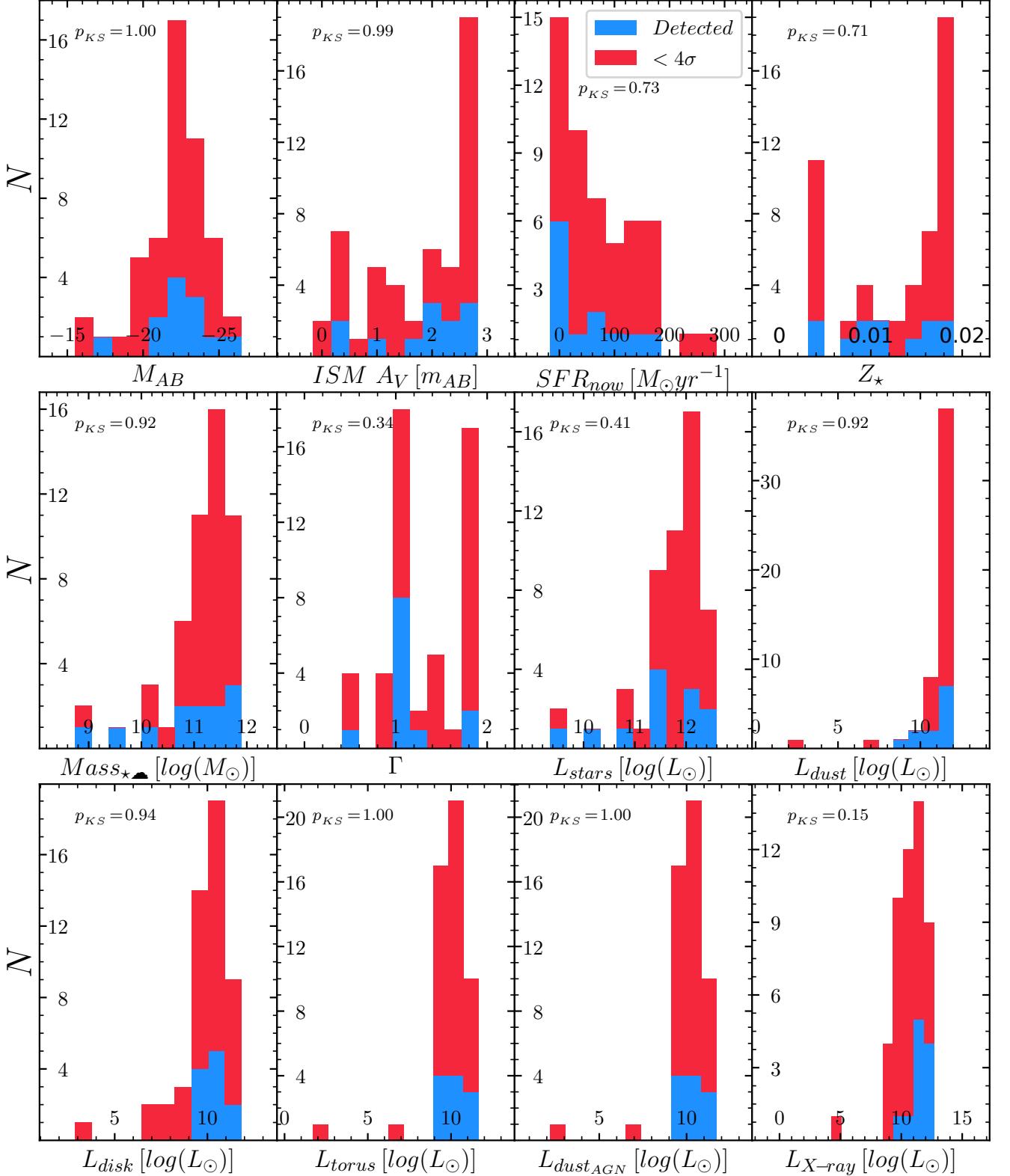


**Figure 1.** SED parameter histograms of the 51 AGN in our sample. Blue bars indicate AGN with a  $\geq 4\sigma$  LyC SNR measurement, and red bars represent  $< 4\sigma$ . K-S test of the two histograms cannot reject the null-hypothesis in any histogram. The  $M_{AB}$  is calculated from the best-fitting CIGALE SED at  $\lambda_{rest} = 1450\text{\AA}$  (e.g., Kulkarni et al. 2019).  $A_V$  is taken from the `Av_ISM` parameter of the attenuation component,  $SFR_{now}$  is from `sfr` in `sfh`,  $Z$  is from metallicity in `stellar`,  $Mass_{\star,\text{sum}}$  is the sum of `m_gas_old`, `m_gas_young`, `m_star_old`, and `m_star_young` in `stellar`,  $\Gamma$  is from `gam` in `xray`,  $L_{stars}$  is the sum of `lum_old` and `lum_young` from `stellar`,  $L_{dust_{abs}}$  is from luminosity in dust,  $L_{disk}$  is from `disk_luminosity` in `agn`,  $L_{torus}$  is from `torus_dust_luminosity` in `agn`,  $L_{dust_{AGN}}$  is from `total_dust_luminosity` in `agn`, and  $L_{X-ray}$  is the `agn_Lx_total` parameter in the `xray` component.

that were within the footprint of our UV imaging. For each AGN, we further reduced the sample to only include spectra that were deemed the highest quality by the PI of the various spectroscopic surveys (Barger et al. 2003; Steidel et al. 2003; Le Fèvre et al. 2004; Cowie et al. 2004; Szokoly et al. 2004; Vanzella et al. 2006; Reddy et al. 2006; Straughn et al. 2008; Barger et al. 2008; Popesso et al. 2009; Treister et al. 2009; Wuyts et al. 2009; Balestra et al. 2010; Yoshikawa et al. 2010; Hodge et al. 2012; Kurk et al. 2013; Buchner et al. 2014; Hsu et al. 2014; Brightman et al. 2014; Wirth et al. 2015; U et al. 2015; Albareti et al. 2017; Herenz et al. 2017; Inami et al. 2017; Liu et al. 2018; Garilli et al. 2021). We visually inspected the  $\sim 2''.0$  region surrounding the AGN in  $\chi^2$  images (Szalay et al. 1999) we created from all available multi-band *HST* imaging to reject objects with close ( $\lesssim 1''.5$ ) neighboring objects from our sample. This selection criteria left us with a total of 51 AGN, which we list in table 3.

Our sample exhibits a diverse range of AGN spectral features, seen from the photometry retrieved from NED (see §4.1). In total, we found that 35 AGN showed X-ray emission (Chandra or Swift detected), 50 near-IR emitters ( $J$ ,  $H$ , or  $K/K_s$ -band), 49 mid-IR emitters (IRAC, WISE 3.4– $12\mu\text{m}$ , or AKARI S11), 44 far-IR emitters (WISE  $22\mu\text{m}$ , PACS, IRS, MIPS, or AKARI L18W), 8 sub-mm AGN (SPIRE, SHARC2  $350\mu\text{m}$ , or LABOCA  $870\mu\text{m}$ ), 4 microwave AGN (IRAM or AzTEC), and 16 radio AGN (ATCA or VLA).

The diversity of our sample is further exemplified in fig. 1. Here we show distributions of several parameters of the best-fitting CIGALE (Boquien et al. 2019) SEDs (see §4 for a full description of our fitting analysis) with LyC S/N measurements from their respective WFC3/UVIS images of  $\geq 4\sigma$  and  $< 4\sigma$  shown as blue and red bars, respectively. We chose  $4\sigma$  as the detection threshold since the other 39 AGN below  $4\sigma$  showed no obvious LyC flux. The  $M_{AB}$  in the first panel is the monochromatic  $1450\text{\AA}$  luminosity calculated from the best-fitting CIGALE SED by integrating the flux between  $\lambda_{rest} = 1449\text{--}1551\text{\AA}$  (e.g., Kulkarni et al. 2019).

We take the remaining parameters from the physical property estimation variables defined in the CIGALE configuration file. Accordingly, the adopted  $A_V$  is taken from the `Av_ISM` parameter in the attenuation component of the full SED model,  $SFR_{now}$  is defined as the `sfr` in `sfh` component,  $Z$  is the metallicity parameter in `stellar` component,  $Mass_{*,\bullet}$  is taken as the sum of the values `m_gas_old`, `m_gas_young`, `m_star_old`, and `m_star_young` in `stellar` component, the X-ray photon index  $\Gamma$  is the `gam` parameter in the `xray` component,  $L_{stars}$  is equal to the sum of the `lum_old` and `lum_young` parameters from the `stellar` component,  $L_{dust_{abs}}$  is the luminosity absorbed by dust taken from the `luminosity` parameter in the `dust` component,  $L_{disk}$  is the `disk_luminosity` parameter in the `agn` component,  $L_{torus}$  is the `torus_dust_luminosity` parameter in `agn` component,  $L_{dust_{AGN}}$  is the emitted dust luminosity taken from the `total_dust_luminosity` parameter in `agn` component, and  $L_{X-ray}$  is the `agn_Lx_total` param-

eter in the `xray` component. K-S tests of each distribution indicate that the two samples are likely from the same larger sample, as the null hypothesis cannot be rejected. Therefore, high SNR LyC flux emitted from AGN may not be discernable from AGN emitting fainter LyC flux when comparing these parameters.

Our sample consists of a somewhat fainter population of AGN, all fainter than  $M_*$  ( $M_{AB} \simeq -27$ ; see Kulkarni et al. 2019) at the average redshift of  $z \sim 3$ . Their SED fits exhibit dusty, weak-AGN characteristics, with the stellar component being the dominant source of their intrinsic luminosity for  $\sim 35\%$  of the sample, while dust dominates the luminosity for  $\sim 45\%$ . Only  $\sim 4\%$  of the sample has the AGN disk component as their brightest feature. Grazian et al. (2018) and Romano et al. (2019) performed a similar study to our present work on AGN with  $-25.1 \leq M_{UV} \leq -23.3$  and  $-29.0 \leq M_{UV} \leq -26.0$ , respectively. Most of their AGN are brighter than ours, which likely explains the ubiquity of detections amongst their samples. Thus, this work serves as a complement to the study of more luminous quasar LyC detections, which do not include LyC non-detected AGN. Their escape fractions are also much higher than the present sample, even for our LyC-detected AGN (see §1), with the lowest  $f_{esc} = 44\%$  from the Grazian et al. (2018) sample. Compared to the Wang et al. (2023) galaxy sample, 19/51 AGN host-galaxies lie in the same range of  $-22 < M_{UV} < -18$ , with four of these being LyC-detected. Here,  $M_{UV}$  is the monochromatic  $1500\text{\AA}$  absolute magnitude calculated from the best-fit CIGALE SEDs, excluding the AGN components. Eight AGN host-galaxies are brighter than  $-22\text{ Mag}$ , two of which are LyC-detected, and 24 are fainter than  $-18\text{ Mag}$ , six of which are LyC-detected. This likely indicates that the AGN itself is emitting most of the detected LyC rather than the host-galaxy's massive stars. Compared to the Steidel et al. (2018) sample, the monochromatic  $1700\text{\AA}$  luminosity of the SEDs from our sample without the AGN component mostly fall within the same range of  $L_{UV}/L_{UV}^* < 3$  ( $L_{UV}^* = -21$  for  $z \simeq 3$ ; Reddy & Steidel 2009). However, we find that 7/51 AGN host-galaxy stellar components exceed this ratio, by an order of magnitude in three cases. Two of these were detected in LyC, namely S-CANDELS J123714.30+621208.5 and WISEA J123623.00+621526.8, with a ratio of  $\sim 9$  and  $\sim 20$  respectively. WISEA J033209.44-274807.3 had an exceptional  $M_{AB} \simeq -25.13$  for its non-AGN SED components, though it was one of the four bright non-detections.

The X-ray luminosity outshines all other SED components for only  $\sim 16\%$  of the sample, indicative of mostly obscured AGN, and all X-ray detected AGN display a soft photon index ( $\Gamma < 2$ ). The population also shows significant star formation, with 50% of the sources showing a SFR between  $10\text{--}100 M_\odot/\text{yr}$ , and  $\sim 37\%$  at  $\text{SFR} > 100 M_\odot/\text{yr}$ , with only the remaining 10% at  $\text{SFR} < 10 M_\odot/\text{yr}$ . Metallicities are more diverse, with  $\sim 32\%$  showing  $Z < 0.01$ , and  $\sim 28\%$  having  $Z \geq 0.02$ , and the rest of the sample having  $0.01 \leq Z \leq 0.02$ .

#### 4. SED FITTING

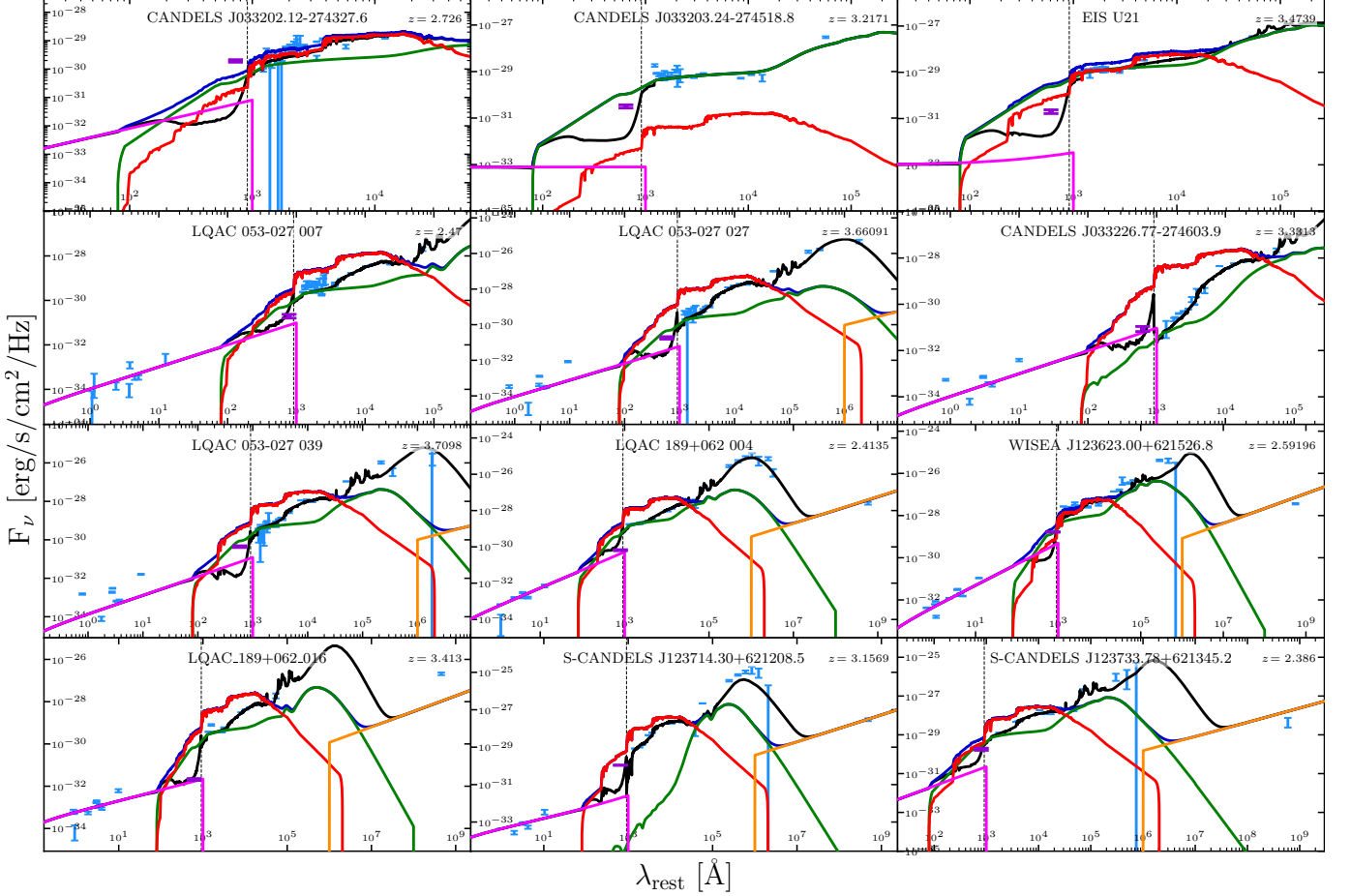


**Figure 2.** CIGALE SED fitting results for the LyC-detected AGN in table 1. The observed photometry is shown as light-blue error bars, and the LyC detection is indicated as a purple error bar. The fitted SED is shown as a black curve, and the blue curve, used for estimating the escape fraction, includes the same SED components as the black curve, excluding all absorption components. The stellar component is shown as the red curve, the AGN component is shown as the green curve, the X-ray emission is shown as the magenta curve, and the radio emission is shown as the orange curve.

#### 4.1. Photometry

The photometry used for SED fitting was compiled from region-based queries of the NED database. We compiled all available photometry within  $1''5$  of the centroid of the corresponding  $\chi^2$  image mentioned in §3. This position offset tolerance was chosen so that our query would capture photometry with larger PSFs, e.g., from X-ray and ground-based data. We homogenized the retrieved photometry to units of mJy based on the instrument and band for all available photometric data. We then added the photometric data point with the highest S/N for each band to our photometric catalog if there was more than one measurement for a particular band. We also filtered out photometric bands from our query that did not have available transmission curves to be used for SED fitting.

The resulting photometric catalog included data from the 2.2-m MPG/ESO WFI (B, V, R, and I), 2MASS J & K<sub>s</sub>, AKARI S11 & L18W, ATCA CABB and 1.4 GHz bands, AzTEC 1.16 mm, Blanco/DECam (*g*, *r*, *i*, *z*, and Y), Blanco/MOSAIC-II H- $\alpha$ , CFHT/WIRCam J & K, Chan-

dra, COMBO-17, Gemini/QUIRC H+K, Hale/WIRC J & K<sub>s</sub>, Herschel (PACS and SPIRE), HST (ACS/WFC F435W, F606W, F775W, F814W, and F850LP, WFC3/IR F098M, F105W, F125W, F140W, and F160W, ACS/SBC F150LP, WFPC2 F300W, and NICMOS F110W and F160W), IRAM 1.2 mm and 2.2 mm, LABOCA 870  $\mu$ m, KPNO/Mayall (G and R from Steidel et al. (2003)), SHARC2 350  $\mu$ m, Spitzer (IRAC, IRS, and MIPS), NTT/SOFI (J, H, and K<sub>s</sub>), SDSS *griz*, SCUBA-2 850  $\mu$ m, Subaru/Suprime-Cam (B, V, R, I, and z), Swift, VISTA/VIRCAM (Y, J, H, and K<sub>s</sub>), VLA (L and C-band), VLT/ISAAC (J, H, and K<sub>s</sub>-band), VLT/HAWK-I K<sub>s</sub>, WISE, and XMM-OM (B and V). This was compiled from a large sample of photometric catalogs: Brandt et al. (2001); Wolf, C. et al. (2001); Alexander et al. (2003); Steidel et al. (2003); Abazajian et al. (2004); Chen & Marzke (2004); Cowie et al. (2004); Jahnke et al. (2004); Koekemoer et al. (2004); Le Fèvre et al. (2004); Smail et al. (2004); Wirth et al. (2004); Wolf et al. (2004); Akiyama (2005); Borys et al. (2005); Bouwens et al. (2005); Pope et al. (2005); Rigby et al. (2005); Thompson et al.

**Table 1.** Individual LyC Detections

ID (1)	$z$ (2)	$m_{\text{LyC}}$ [ $m_{AB}$ ] (3)	$\text{SNR}_{\text{LyC}}$ (4)	$f_{\text{esc}}$ [%] (5)	$m_{\text{UVC}}$ [ $m_{AB}$ ] (6)
CANDELS J033202.12-274327.6	2.726	25.68±0.11	10.04	227±83.5	25.65±0.04
CANDELS J033203.24-274518.8	3.2171	27.64±0.17	6.27	17±6.7	24.82±0.01
EIS U21	3.4739	28.14±0.20	5.41	5±1.6	24.14±0.00
LQAC 053-027 007	2.47	28.16±0.21	5.21	7±2.4	25.75±0.01
LQAC 053-027 027	3.6609	28.24±0.17	6.25	1 <sup>+8.1</sup> <sub>-1</sub>	25.69±0.02
CANDELS J033226.77-274603.9	3.3313	29.04±0.27	3.99	4 <sup>+29.2</sup> <sub>-4</sub>	27.23±0.15
LQAC 053-027 039	3.7098	27.28±0.11	9.71	7 <sup>+44.2</sup> <sub>-7</sub>	24.85±0.01
LQAC 189+062 004	2.4135	26.86±0.07	16.06	3 <sup>+13.4</sup> <sub>-3</sub>	23.66±0.00
WISEA J123623.00+621526.8	2.592	23.35±0.00	585.77	65±2.6	20.77±0.00
LQAC 189+062 016	3.413	30.60±0.11	9.88	2±6.9	26.42±0.01
S-CANDELS J123714.30+621208.5	3.1569	26.31±0.00	375.68	101±9.0	25.97±0.01
S-CANDELS J123733.78+621345.2	2.386	25.75±0.14	7.72	12 <sup>+124.7</sup> <sub>-12</sub>	23.66±0.01

NOTE—**Table columns:** (1) NED object ID; (2) AGN spectroscopic redshift; (3) LyC AB magnitude measured in the corresponding WFC3/UVIS filter; (4) S/N of measured LyC flux; (5) The  $f_{\text{esc}}$  of the AGN and host-galaxy and its uncertainties. Values over 100% are included to show the limitations of the SED models.; (6) The non-ionizing UV AB magnitude measured from the ACS/WFC F606W filter.

(2005); Afonso et al. (2006); Alonso-Herrero et al. (2006); Beckwith et al. (2006); Biggs & Ivison (2006); Coe et al. (2006); Kovács et al. (2006); Laird et al. (2006); Reddy et al. (2006); Steffen et al. (2006); Weiner et al. (2006); Kelly et al. (2007); Rodighiero et al. (2007); Adelman-McCarthy et al. (2008); Aird et al. (2008); Cardamone et al. (2008); Finkelstein et al. (2008); Kellermann et al. (2008); Mainieri et al. (2008); Miller et al. (2008); Wiklind et al. (2008); Wuyts et al. (2008); Chen & Shan (2009); Daddi et al. (2009); Mancini et al. (2009); Negrello et al. (2009); Rigopoulou et al. (2009); Treister et al. (2009); Young et al. (2009); Carilli et al. (2010); Lutz et al. (2010); Morrison et al. (2010); Pearson et al. (2010); Cameron et al. (2011); Georgantopoulos et al. (2011); Magnelli et al. (2011); Penner et al. (2011); Puccetti et al. (2011); Reis et al. (2011); Shim et al. (2011); Teplitz et al. (2011); Vagnetti et al. (2011); Cutri et al. (2013); Bizzocchi et al. (2014); Bouwens et al. (2014); Cutri et al. (2014); Huang et al. (2014); Skelton et al. (2014); Straatman et al. (2014); Tan et al. (2014); Antonucci et al. (2015); Ashby et al. (2015); Franzen et al. (2015); Falocco et al. (2015); Huynh et al. (2015); Jiménez-Teja et al. (2015); Capelluti et al. (2016); Harikane et al. (2016); Wang et al. (2016); Xue et al. (2016); Cowie et al. (2017); Guidetti et al. (2017); Tie et al. (2017); Liu et al. (2018); Vito et al. (2018). All of these catalogs were used for SED fitting for at least one AGN, but not all AGN had photometry taken from every catalog. The brightest band and its flux in each part of the AGN emission spectrum is listed in the Appendix table 3.

#### 4.2. CIGALE Configuration

We used the CIGALE (Boquien et al. 2019) SED fitting code to model the AGN emission from X-ray to radio wavelengths. These models enable us to calculate the intrinsically produced LyC of the AGN and host-galaxy.

We used the `sfhdelayedbq` model and `bc03` templates to model the star-formation history and stellar populations, nebular templates to simulate emission lines from the ISM, `dustatt_modified_CF00` model to simulate dust attenuation, `skirtor2016` templates to fit the AGN emission, `dale2014` templates to simulate the thermal dust emission, `xray` model to simulate the X-ray emission from stars and the AGN, and the `radio` module model to simulate the galaxy synchrotron and AGN emission during fitting.

These components are a combination of mathematical models with free parameters and templates with pre-defined choices of parameters, i.e. the `bc03`, nebular, `dale2014`, and `skirtor2016` templates. All but the `dale2014` templates, however, are in-turn based on physically motivated, empirical mathematical models (Ferland et al. 1998, 2013; Bruzual & Charlot 2003; Stalevski et al. 2012, 2016). These templates, of course, limit the parameter space by the resolution and range of the parameters in the templates provided by CIGALE. Incorporating additional models not included in the main distribution of CIGALE could improve this. Another limitation we observed comes from how the nebular component scales the LyC to provide energy to emission lines. When the observed LyC flux exceeds the modeled LyC flux (which includes a wavelength-dependent IGM attenuation factor at redshift  $z$ ), the nebular LyC scaling may produce erroneous results. This case can occur for high  $f_{\text{esc}}$  galaxies and AGN, since higher  $f_{\text{esc}}$  values have likely been observed through lines-of-sight with higher than average IGM transmission. When including photometry below the rest-frame Lyman-limit, the modeled LyC gets scaled to meet this observed LyC flux, creating an unphysical “jump” or discontinuity at 912 Å. To circumvent this, we did not fit any SEDs to photometry measured at rest-frame wavelengths shorter than 1216 Å.

We also modified the code to extrapolate the power law fit of the X-ray model to 1000 Å specifically for our AGN since the AGN continuum power-law shows a break at around this wavelength (Telfer et al. 2002), and also to fill the discontinuity in the model between  $220 \lesssim \text{Å} \lesssim 400$  that exists without this modification. This will also account for the hard UV tail of the AGN warm corona emission (e.g., Lusso et al. 2015; Petrucci et al. 2020).

## 5. LYC PHOTOMETRY AND ESCAPE FRACTIONS

We performed all LyC photometry as we have in our previous LyC work from S18 and S20. In summary, we treat each pixel as a random variable with normally distributed flux, where the mean is set to the pixel value from the drizzled science image, and the dispersion is set to the RMS value from the corresponding pixel in the weightmap, plus the local sky dispersion measured in the  $151 \times 151$  pixels ( $4''.53 \times 4''.54$ ) surrounding the target, normalized to each individual pixel. Neighboring object pixels were also masked in this process. We then generated 10,000 randomly drawn  $151 \times 151$  pixel images using these statistics, and measured the flux within the Kron-like elliptical aperture detected from the  $\chi^2$  image for each realized image (created using all available *HST* data; see Szalay et al. 1999) using SExtractor (Bertin & Arnouts 1996). The resulting flux distribution from these measurements was used to determine the LyC flux and its uncertainties given in table 1. When performing photometric measurements on our LyC stacks (see §5.1 for details on our stacking procedure), we treated each pixel in each sub-image of a stack as a random variable which creates a  $151 \times 151 \times 10,000$  data cube for that sub-image, then stacked each data cube using a weighted sum. We then normalized the stack of data cubes by a stack of all weightmap cutouts. The flux distribution was then generated in the same way as the individually detected AGN, taking slices from the data cube and measuring the central isophotal flux, using the  $\chi^2$  image for detection. The resulting stacked photometry and its uncertainties is presented in more detail §5.1 and table 2.

To calculate the LyC  $f_{\text{esc}}$ , we used the same method as in S18 and S20. In our method, we simply take the ratio of the observed LyC flux to an intrinsic LyC flux modelled using the unattenuated SED, the WFC3/UVIS filter curve corresponding to the observed LyC flux filter, and IGM attenuation curves modeled at the redshift of the target AGN. In short, we modeled the intrinsic LyC flux from the best-fitting CIGALE SED using only the following components: stellar.old, stellar.young, nebular.lines.young, nebular.lines.old, nebular.continuum.young, nebular.continuum.old, agn.SKIRTOR2016\_disk, agn.SKIRTOR2016\_torus, agn.SKIRTOR2016\_polar\_dust, xray.galaxy, xray.agn, radio.sf.nonthermal, and radio.agn. We summed these components to acquire our intrinsic SED, then we calculated the inner product of this SED with the IGM attenuation curves and filter transmission curves to obtain our final intrinsic LyC flux model. We performed this inner

product 10,000 times for the variety of sight-lines through the IGM at the redshift of the AGN using the model from Inoue et al. (2014). We used the flux distribution described in the previous paragraph as the observed LyC flux, took the ratio of these two distributions, and used this ratio to calculate the  $f_{\text{esc}}$  distribution and its statistics which are presented in table 1. It is worth noting that the modeled LyC from the SED, as well as the apertures shown in Fig 3 are intended to capture both the LyC emission from the central AGN as well as any stellar LyC leaking from the host galaxy.

We find a wide range of  $f_{\text{esc}}$  values from 1–100% or greater, which represent the mode of the  $f_{\text{esc}}$  distribution. Corresponding  $1\sigma$  uncertainties, along with the  $f_{\text{esc}}$  values are shown in Table 1. An inverse variance weighted average value including all values in Table 1 (with a ceiling of 100%) equates to approximately  $f_{\text{esc}} \simeq 18\%$ .  $f_{\text{esc}}$  distributions with modes above 100% result from higher observed LyC compared to the modeled, intrinsic LyC obtained from the best-fit CIGALE SED. Although these  $f_{\text{esc}}$  values are unphysical, and at a  $\sim 2.7\sigma$  significance, we show the  $f_{\text{esc}}$  in these cases to highlight the need for AGN models that can accommodate high LyC emission.

### 5.1. LyC Stacking

Stacking is a technique generally used to increase the SNR of signals from sources of interest, or to find the average signal of a sample. In this work, we stack LyC flux from galaxies hosting AGN to compare the total LyC signal brightness of various subsets within our sample based on observed spectral features. To distinguish these subsets, we used the archival photometry retrieved from the various catalogs hosted on Vizier and categorized the detected photometric bands into regions of the electromagnetic spectrum, namely X-ray, optical, IR, MIR, FIR, sub-mm, microwave, and radio. We did not include a UV-detected sample since U-band may overlap with the rest-frame LyC for some higher- $z$  AGN. Each of these subsamples is defined by having a detection in their respective region of the EM spectrum. The bandpass filters used for determining the inclusion in each subsample can be found in §4.1.

We show the resulting stacks of galaxies in each band in fig. 4, and the photometry performed for each stack is presented in table 2. We find the stack with the brightest LyC emission is the sub-mm detected AGN in the F336W stack, with redshifts that range from  $3.15 < z < 3.71$ . There are only three objects in this stack, so it is likely there is a detection bias since detection in sub-mm often implies overall brighter luminosity across the SED. The LyC stack of all AGN detected in a particular region of the electromagnetic spectrum was the IR- and MIR-detected AGN LyC stacks, which includes 50 and 49 out of the 51 AGN, respectively. The AGN missing from these stacks simply did not have any IR/MIR band observations. A zero-point normalized stack (the “All LyC” row in the All AGN set of stacks in table 2) was brighter than these two stacks, and includes all 51 AGN. We also stack the LyC non-detections in each of our three

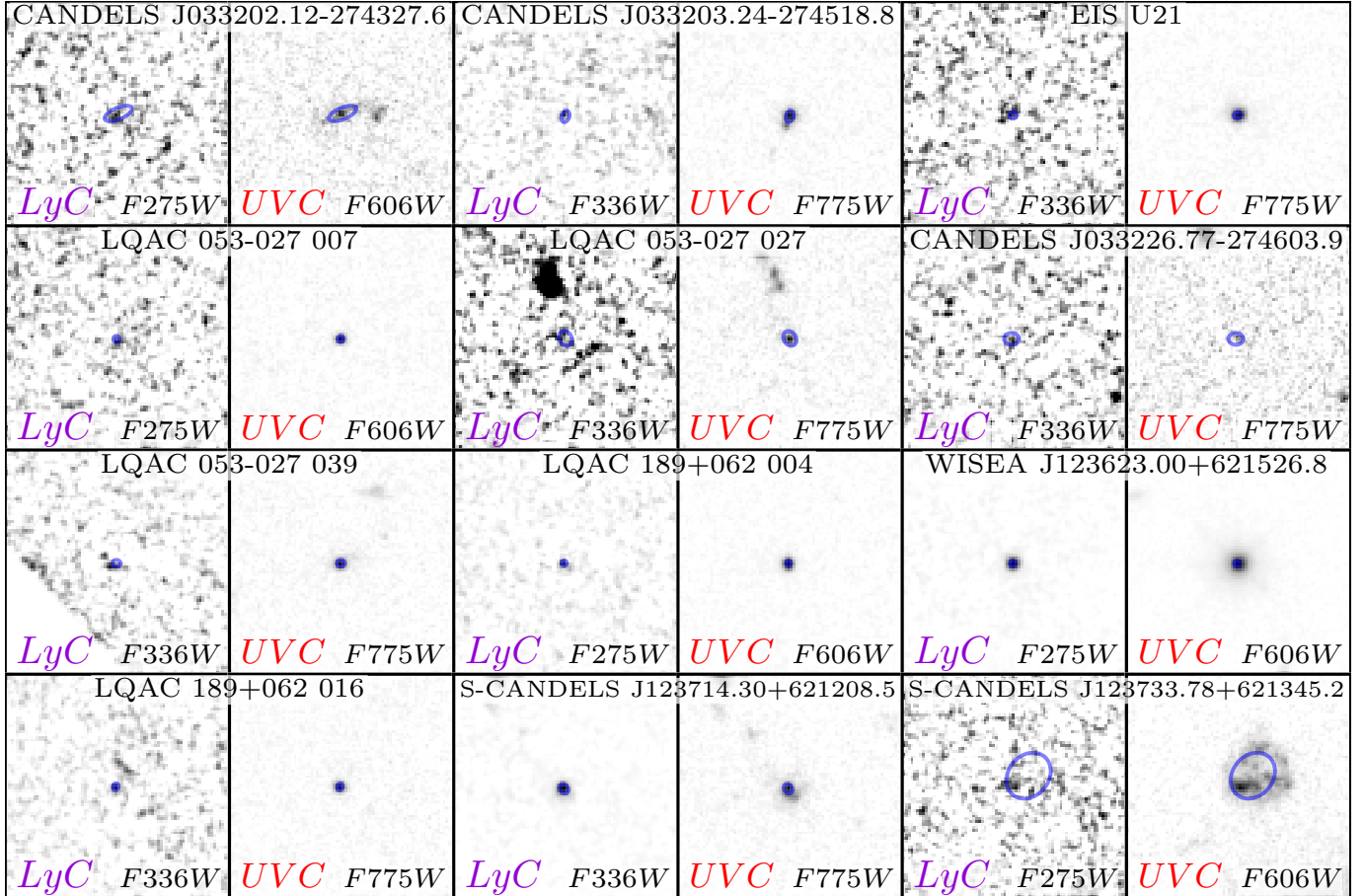


**Figure 3.**  $4''.53 \times 4''.53$  cutouts of our LyC detected AGN showing their LyC image (LyC, left) and  $\sim 1500\text{\AA}$  rest-frame UV continuum (UVC, right). The NED object name and corresponding filters are also shown. The  $\chi^2$  image detected apertures are shown as blue ellipses.

redshift bins, as well as a stack of all non-detections. None of these stacks resulted in detected LyC.

These results demonstrate that stacks based on detected regions in the AGN electromagnetic continuum do not correlate well with their LyC emission. There are many factors that can affect the LyC flux that is detected, e.g., sample size statistics, IGM line of sight attenuation, AGN inclination, observed filter and its proximity to the Lyman-limit, or other intrinsic physical factors of the host-galaxy or AGN. A correlation analysis on an individual basis of each AGN's LyC emission may reveal more clues for which regions of the continuum could indicate LyC leakage.

We also created stacks based on the filter-cutoff's proximity to the AGN's observed-frame Lyman-limit. We stacked the LyC cutouts in two redshift bins (low- $z$  and high- $z$ ) separated by their median redshift for four samples in the “All AGN” set of stacks, i.e., the F225W, F275W, F336W, and “All” samples. In all cases, we see that the low- $z$  substacks, which would have their Lyman-limit closer to the filter cutoff, show brighter LyC emission than the high- $z$  substacks. This result is not surprising since a given filter would observe shorter wavelength flux for higher redshift galaxies, and the central AGN and stellar sources produce less LyC flux further from the Lyman-limit. From this, we conclude

that LyC observations should attempt to select targets with Lyman-limits as close as possible to their filter-cutoffs, while minimizing red-leak in the filter beyond the Lyman-limit below some fiducially low percentage.

Of the stacks based on redshift ranges which correspond to observed WFC3/UVIS F225W, F275W, and F336W filters, we find that the stack of all galaxies in the F336W sample ( $3.08 < z < 4.88$  ( $z$ )  $\sim 3.5924$ ) containing 16 AGN was the brightest substack with  $m_{AB} = 27.66 \pm 0.56$ . This result is more interesting, since the higher redshift AGN should experience more attenuation from the IGM. Furthermore, AGN activity peaks at  $z \sim 2-3$  in space-density and  $M_*$  (Kulkarni et al. 2019), and AGN in this stack are expected to be intrinsically fainter. Since AGN do not exhibit evolution in their SED through redshift (e.g., Barth et al. 2003; Fan et al. 2004; Iwamuro et al. 2004; Jiang et al. 2007), the LyC emission from AGN may not be redshift dependent either. Thus, it is more likely the case that LyC emission from AGN is solely dependent on physical parameters of the AGN and host-galaxy, or inhibited to some degree by the surrounding IGM.

## 6. RESULTS

**Table 2.** Lyman Continuum Stack Photometry

Filter	$z$ -range	$\langle z \rangle$	$N_{obj}$	$m_{LyC}$	$ABerr_{LyC}$	$S/N_{LyC}$	$A_{UVC}$	$m_{UVC}$	$ABerr_{UVC}$
(1)	(2)	(3)	(4)	(5)	(6)	(7)	(8)	(9)	(10)
<b>ALL AGN:</b>									
F225W	2.2807-2.2979	2.2893	2	>27.01	...	(1.0) $^{\ddagger}$	1.28	25.626	0.024
F225W (low- $z$ )	2.2807-2.2807	2.2807	1	>29.26	...	(1.0) $^{\ddagger}$	0.19	27.994	0.112
F225W (high- $z$ )	2.2979-2.2979	2.2979	1	>26.92	...	(1.0) $^{\ddagger}$	1.27	25.017	0.019
F275W	2.3860-3.0750	2.6117	33	28.83	0.62	1.75	0.57	23.314	0.000
F275W (low- $z$ )	2.3860-2.7280	2.5324	26	28.19	0.56	1.95	0.98	23.654	0.001
F275W (high- $z$ )	2.7370-3.0750	2.9062	7	>29.29	...	(1.0) $^{\ddagger}$	0.20	22.681	0.000
F336W	3.0804-4.8759	3.5924	16	27.66	0.56	1.95	0.50	24.941	0.004
F336W (low- $z$ )	3.0804-3.9050	3.4445	14	29.07	0.31	3.53	0.46	24.876	0.004
F336W (high- $z$ )	4.3792-4.8759	4.6275	2	>28.95	...	(1.0) $^{\ddagger}$	0.57	25.878	0.031
All LyC	2.2807-4.8759	2.9067	51	28.46	0.45	2.39	0.54	23.874	0.001
All LyC (low- $z$ )	2.2807-3.9050	2.8377	41	30.51	0.55	1.96	0.84	24.252	0.001
All LyC (high- $z$ )	2.2979-4.8759	3.1896	10	>29.09	...	(1.0) $^{\ddagger}$	0.21	23.053	0.000
<b>LYC NON-DETECTIONS:</b>									
F225W	2.2807-2.2979	2.2893	2	>27.01	...	(1.0) $^{\ddagger}$	1.28	25.626	0.024
F275W	2.4030-3.0750	2.6285	28	>28.41	...	(1.0) $^{\ddagger}$	0.87	23.730	0.001
F336W	3.0804-4.8759	3.7239	9	27.93	0.47	2.31	0.28	25.437	0.007
All LyC	2.2807-4.8759	2.8639	39	28.83	0.91	1.20	0.89	24.121	0.001
<b>XRAY DETECTED:</b>									
F225W	2.2807-2.2979	2.2893	2	>26.95	...	(1.0) $^{\ddagger}$	1.34	25.623	0.024
F275W	2.4135-3.0750	2.6613	21	>29.16	...	(1.0) $^{\ddagger}$	0.18	22.943	0.000
F336W	3.0804-4.8759	3.5972	12	27.89	0.77	1.42	0.50	25.033	0.005
All LyC	2.2807-4.8759	2.9609	35	29.47	0.78	1.39	0.21	23.613	0.000
<b>IR DETECTED:</b>									
F225W	2.2807-2.2979	2.2893	2	>27.15	...	(1.0) $^{\ddagger}$	1.24	25.662	0.024
F275W	2.3860-3.0750	2.6105	32	28.93	0.72	1.51	0.56	23.304	0.000
F336W	3.0804-4.8759	3.5924	16	27.51	0.36	3.01	0.49	24.949	0.004
All LyC	2.2807-4.8759	2.9119	50	28.66	0.54	2.03	0.55	23.869	0.001
<b>MIR DETECTED:</b>									
F225W	2.2807-2.2979	2.2893	2	>27.14	...	(1.0) $^{\ddagger}$	1.24	25.666	0.024
F275W	2.3860-3.0750	2.6104	32	29.09	0.81	1.35	0.57	23.282	0.000
F336W	3.0804-4.8759	3.5842	15	27.73	0.52	2.10	0.52	24.878	0.004
All LyC	2.2807-4.8759	2.8954	49	28.66	0.62	1.75	0.55	23.835	0.001
<b>FIR DETECTED:</b>									
F225W	2.2807-2.2979	2.2893	2	>27.05	...	(1.0) $^{\ddagger}$	1.20	25.716	0.025
F275W	2.3860-3.0750	2.6199	29	>28.84	...	(1.0) $^{\ddagger}$	0.55	23.181	0.000
F336W	3.0804-4.3792	3.4926	13	27.60	0.43	2.55	0.53	24.795	0.004
All LyC	2.2807-4.3792	2.8627	44	29.04	0.78	1.39	0.56	23.734	0.001
<b>SUB-MM:</b>									
F225W	2.2807-2.2979	2.2893	2	>27.12	...	(1.0) $^{\ddagger}$	1.23	25.640	0.023
F275W	2.4030-3.0750	2.6551	5	27.45	0.28	3.94	0.28	24.058	0.002
F336W	3.1569-3.7098	3.5069	3	26.95	0.44	2.45	0.56	24.175	0.005
All LyC	2.4030-3.7098	2.9745	8	29.94	0.41	2.66	0.37	24.442	0.002
<b>MICROWAVE DETECTED:</b>									
F225W	2.2807-2.2979	2.2893	2	>27.12	...	(1.0) $^{\ddagger}$	1.23	25.640	0.023
F275W	2.4030-3.0750	2.6305	3	27.61	0.49	2.23	0.28	23.500	0.001
F336W	3.9050-3.9050	3.9050	1	>28.19	...	(1.0) $^{\ddagger}$	0.15	26.543	0.038
All LyC	2.4030-3.9050	2.9491	4	30.17	0.44	2.45	0.27	24.045	0.002
<b>RADIO DETECTED:</b>									
F225W	2.2807-2.2979	2.2893	2	>27.12	...	(1.0) $^{\ddagger}$	1.23	25.640	0.023
F275W	2.3860-3.0750	2.5986	12	>28.61	...	(1.0) $^{\ddagger}$	0.24	22.838	0.000
F336W	3.1569-3.6609	3.4712	4	27.62	0.54	2.00	0.51	24.437	0.005
All LyC	2.3860-3.6609	2.8167	16	>30.78	...	(1.0) $^{\ddagger}$	0.26	23.268	0.000

**NOTE—Table columns:** (1) Observed WFC3/UVIS filter; (2) Redshift range of galaxies included in LyC/UVC stacks. Overlapping ranges for the low- and high- $z$  “All” samples are due to splitting the F225W, F275W, and F336W samples by their median redshift before combining the three subsamples into either the high- or low- $z$  “All” sample; (3) Average redshift of all galaxies in each stack; (4) Number of galaxies with reliable spectroscopic redshifts included in each stack; (5) Observed total AB magnitude of LyC emission from stack (SEXTRACTOR MAG\_AUTO) aperture matched to UVC, indicated by the blue ellipses in figs. X-Y; (6)  $1\sigma$  uncertainty in LyC AB-mag; (7) Measured S/N of the LyC stack flux ( $\dagger$  indicates a  $1\sigma$  upper limit); (8) Area (in arcsec $^2$ ) of the UVC aperture; (9) Observed total AB magnitude of the UVC stack; (10)  $1\sigma$  uncertainties of UVC AB-mag. Listed uncertainties do not include systematic filter zeropoint uncertainty, which are  $< 2-4\%$  (Windhorst et al. 2022; O’Brien et al. 2023).

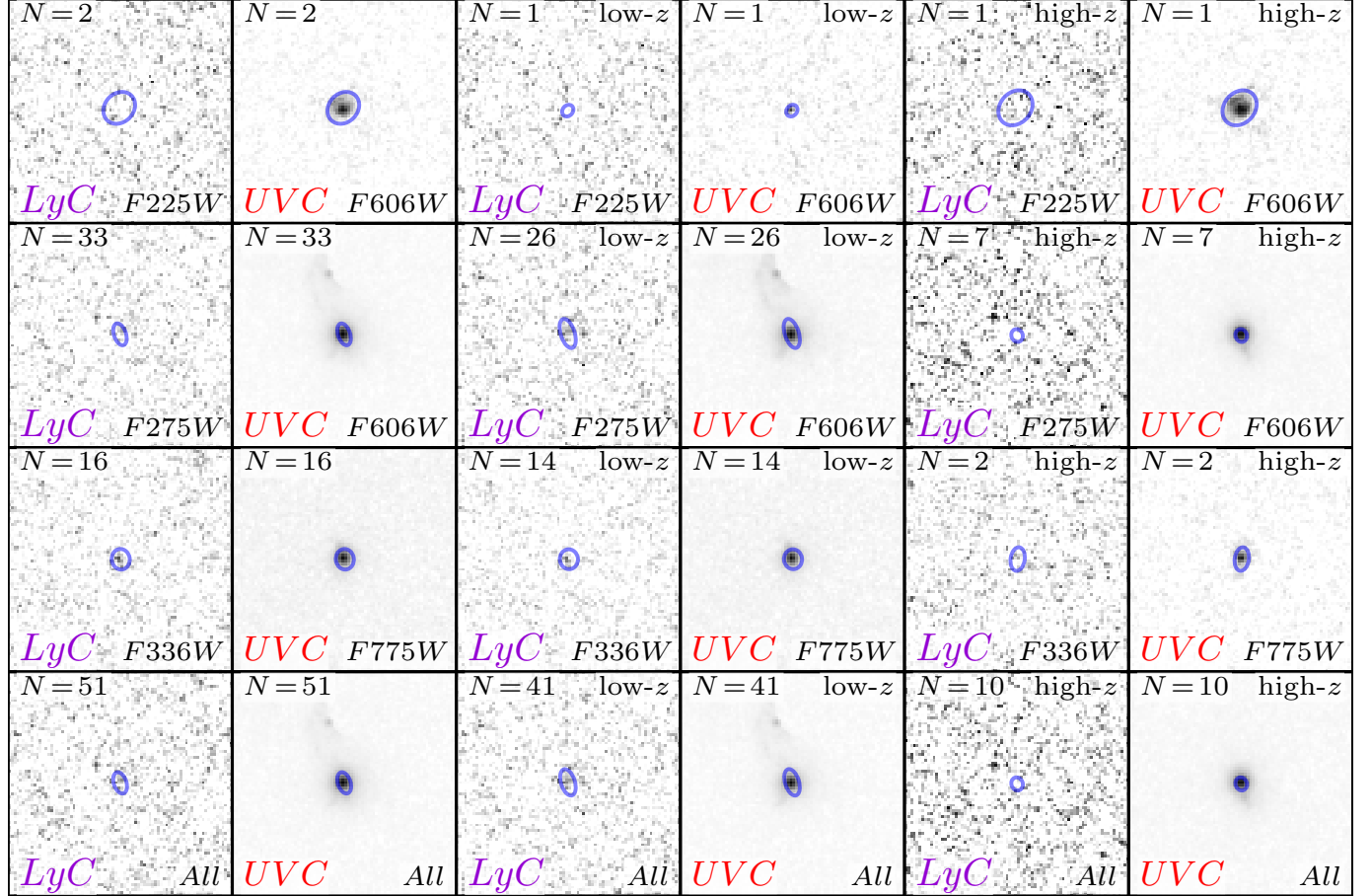


**Figure 4.** LyC and UVC stacks of all AGN in the total sample. Blue ellipses are SExtractor detection apertures from the UVC stack. The number of AGN included in each stack is indicated on the top-left corner of each individual panel. Left two columns show the full sample of AGN where LyC can be measured in either the filter indicated on the bottom right of the panel, or the total AGN (“All”) sample in the bottom row. The middle and right pair of columns represent half of the AGN in their row, split into low and high redshift samples using the average redshift of the sub-sample as a separator. Top row: AGN with LyC measurable in F225W; Top-middle row: same but for F275W; Top-bottom row: same but for F336W; Bottom row: Same, but for all AGN in the total sample.

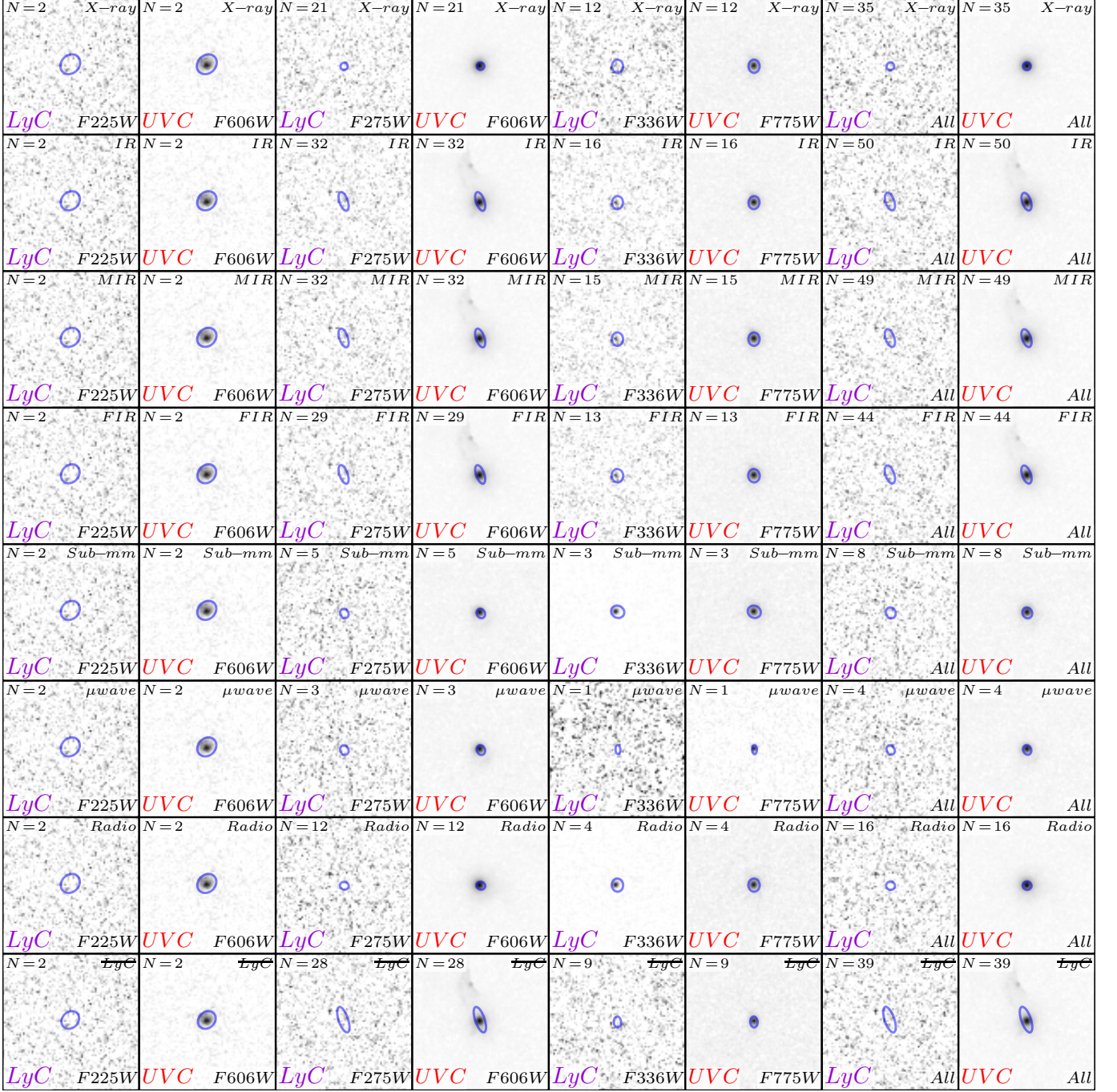


**Figure 5.** LyC and UVC stacks of AGN sub-samples listed in table 2. Top row: Sub-sample of AGN that were detected by Chandra and/or Swift; 2nd row: AGN detected in an IR band (J, H, or K); 3rd row: AGN detected in a Mid-IR band (IRAC, WISE 3.4–12 $\mu$ m, or AKARI S11); 4th row: AGN detected in a Far-IR band (WISE 22 $\mu$ m, PACS, IRS, MIPS, or AKARI L18W); 5th row: AGN detected in a sub-mm band (SPIRE, SHARC2 350  $\mu$ m, or LABOCA 870  $\mu$ m); 6th row: AGN detected in the microwave region (IRAM or AzTEC); 7th row: AGN detected in the radio (ATCA or VLA). Bottom row: LyC non-detected AGN, indicated by  $\text{LyC}^{\text{C}}$ . The IR-detected AGN show the brightest flux among the "All" sub-samples, with 39 included in the stack. The brightest sub-sample of all panels is the F336W IR-detected sub-sample.

As seen in §3, our AGN with LyC flux detected at  $>4\sigma$  and those with LyC measured below  $4\sigma$  are most likely not distinct samples when considering the SED parameters we used for characterization. In order to ascertain some parameter dependence on the LyC flux, we computed the Pearson cor-

relation coefficient between LyC flux, including upper limits, and several SED parameters, namely the  $M_{AB}$ , stellar mass, the ISM  $A_V$ , metallicity, the instantaneous star-formation rate, the ionization parameter  $U$ , the X-ray photon index, the AGN inclination, and the luminosities of the young, old,

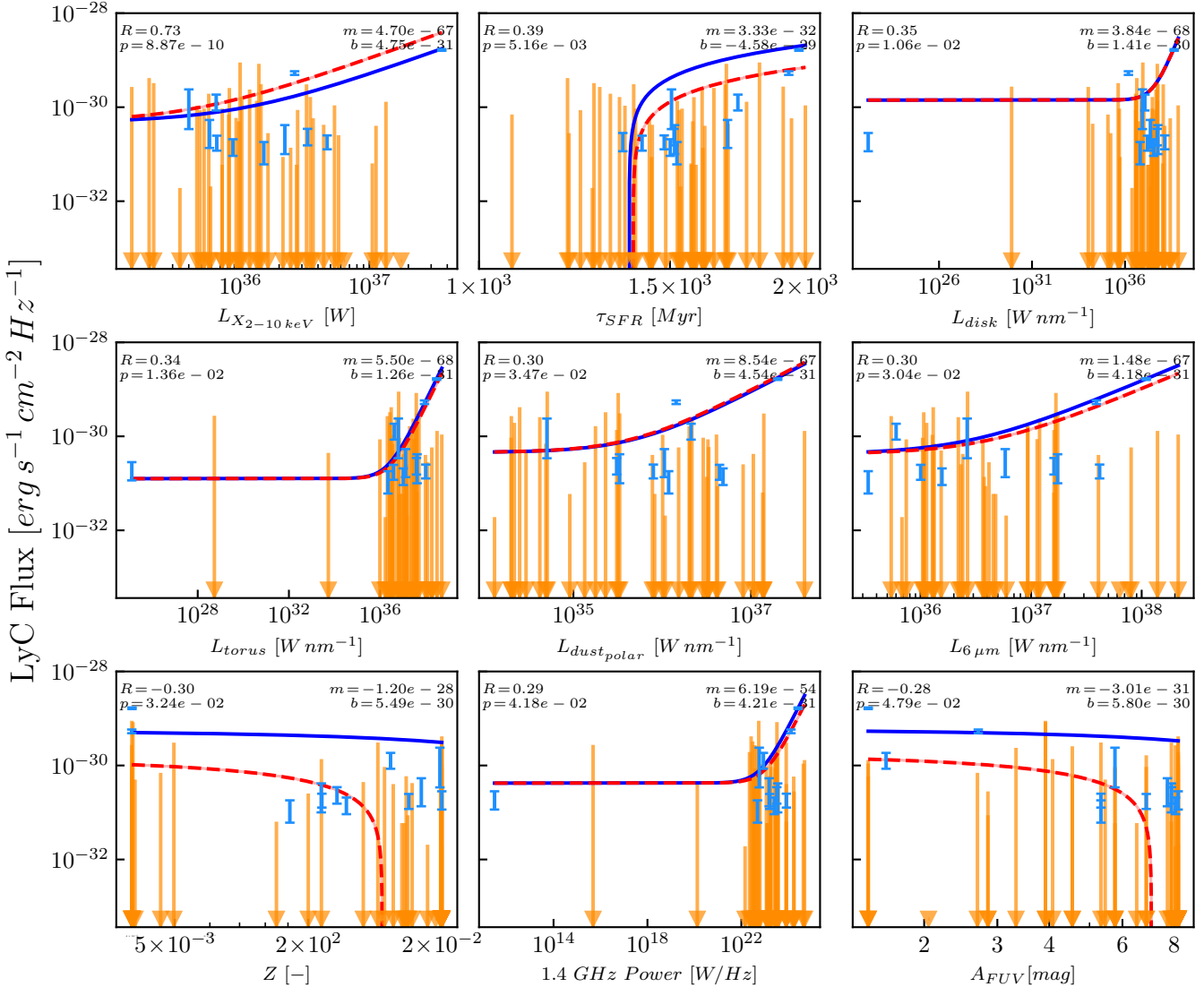


**Figure 6.** Lyman continuum flux vs. various best-fitting SED parameters with strong correlations for our AGN sample. Light-blue points indicate detected LyC while orange bars are  $1\sigma$  upperlimits to the LyC flux. The dark blue line is the Bayesian fit to the data with slope and intercept shown ( $m$  and  $b$ , respectively), treating upper limits as censored and the red-dashed line is the same fit, excluding the brightest point with the largest weight. Despite this exclusion, the general trends still survive. All correlation coefficients “ $R$ ” shown reject the null-hypothesis ( $p < 0.05$ ). The strongest correlating parameter is the X-ray luminosity from 2–10 keV, indicating a strong X-ray to LyC emission connection for AGN. The SFH  $\tau$  onset age parameter shows strong correlation, which implies higher LyC emission after more recent star-formation episodes. Several dust parameters (torus dust luminosity, polar dust luminosity,  $6\mu\text{m}$  luminosity, and  $A_{FUV}$ ) show strong correlation with LyC flux, as well as 1.4 GHz radio emission. Stellar metallicity shows a strong anti-correlation to LyC flux, which may signify a preference for higher LyC emission from metal poor galaxies.

and young+old stellar populations, the AGN disk, the AGN dust torus, AGN polar dust, the disk+torus+polar dust, the ISM dust, and the X-ray emission. Since our LyC photometric data is composed of mostly upper limits, the LyC flux is most appropriate to correlate parameters to, since scaling the UV skybackground to high redshift luminosity would only increase the uncertainty in the data. Furthermore, flux correlations can inform future searches for AGN LyC leaker *detections* in imaging.

We found the parameter with the strongest correlation was best fitting AGN SED 2–10 keV X-ray luminosity, with  $r \simeq 0.73$  and  $p \simeq 8.86 \times 10^{-10}$ . The next strongest correlation was main stellar population’s star-formation onset age  $\tau$  ( $r, p \simeq (0.39, 5.16 \times 10^{-3})$ ), assuming the delayed “burst-quench” model of Ciesla et al. (2017). The remaining significant positive correlation coefficients in decreasing strengths are the AGN disk luminosity ( $r, p \simeq (0.35, 0.011)$ ), AGN torus luminosity ( $r, p \simeq (0.34, 0.014)$ ), the AGN

monochromatic  $6\mu\text{m}$  luminosity ( $r, p \simeq (0.30, 0.030)$ ), then the AGN 1.4 GHz power ( $r, p \simeq (0.29, 0.042)$ ). We find a weak correlation to stellar luminosity, but this was not statistically significant ( $p \simeq 0.19$ ), which was stronger for the older stellar population ( $p \simeq 0.10$ ) compared to the younger population. We also find significant anti-correlation to the metallicity of the stellar component SED with  $r, p \simeq (-0.30, 0.032)$  and  $A_{FUV}$  ( $r, p \simeq (-0.28, 0.048)$ ). We find no correlation to the AGN fraction parameter or X-ray photon index.

In fig. 6, we show LyC flux vs. these parameters along with a Bayesian fit to the data. We used normal distributions to model the LyC flux probability for data with  $\text{S/N} > 1\sigma$ , and treat the LyC flux with  $\text{S/N} < 1\sigma$  as censored data, modelling these data using arbitrary probability distributions while constraining the log-cumulative distribution function to the  $1\sigma$  uncertainty of the observed LyC flux. Since the points with highest SNR have the most weight in these fits, we also fit a line to the data excluding the point with the highest flux (plotted as a dashed-red curve). As shown, this does not have significant impacts on the general direction of these lines, though the curves for metallicity and  $A_{FUV}$  show the most change. Of the eight curves, five are negligibly different, and the curves for  $L_{X_{2-10\text{ keV}}}$  and  $\tau_{SFR}$  are within the uncertainty ranges of the data. The p-values are generally higher without this bright point, which indicates that these correlations would significantly improve with more LyC-detected AGN included in the analysis.

## 7. DISCUSSION

In general, our results indicate that higher LyC emission can be traced to intrinsically higher LyC production via the AGN accretion disk and host-galaxy stellar sources. We compared subsamples of our AGN split into redshift bins and detected regions of the AGN continuum regions and find no significant distinctions. Our correlation tests show that high-LyC emitting AGN can be found from various markers that might indicate high ionizing photon production, i.e., X-ray and IR/dust emission brightness. X-ray emission from AGN is created as a result of Comptonization of optical/UV photons produced by the accretion disk, which up-scatter off of a corona of hot electrons in close proximity to the SMBH into the X-ray regime (Haardt & Maraschi 1991). A significant fraction of these UV photons will be ionizing, therefore the LyC that is not processed into X-rays can escape the host-galaxy and ionize the IGM. Thus it is not surprising that X-ray luminosity correlates significantly with observed LyC flux.

Some of the X-ray emission is also reprocessed by the dust torus, the broad-line region and the accretion disk. The toroidal and polar dust will become heated by the UV/optical light produced by the accretion disk, giving rise to extinction and luminous IR features in the SED. It is therefore reasonable to predict that brighter LyC production would result in brighter dust emission features, which is what we observed from correlating these parameters. The LyC that is not absorbed or reprocessed by dust will also have some probability

of escaping the host-galaxy, and more flux will be observed if more LyC is produced by the disk. The detected LyC emission may rely on the line of sight or angle at which the AGN is observed.

Stellar sources in the host-galaxy will also contribute to the observed LyC since the accretion disk would mostly saturate LyC absorbers in the ISM and near the SMBH. This is true if the stellar sources can produce LyC in significant amounts, which are typically A, B, and O-type stars. The most massive O-type stars will produce the most LyC, though they typically only live for  $\lesssim 10$  Myr before going supernova,  $\lesssim 200$  Myr for B-types, and several hundred Myr for A-types. Therefore, one would expect that recent star-formation episodes producing newly formed massive stars would increase the observed LyC emitted by galaxies, which is corroborated by our correlation results. Furthermore, metal poor stars should produce more LyC than more metal rich stars since the photospheres would absorb less of the high energy ionizing light, which we also observe in our correlation analysis.

We therefore infer that AGN with detectable LyC flux would be those with bright X-ray or thermal dust emission, with additional flux coming from the host-galaxy stellar population produced within a few Myrs of a star formation episode that produced lower metallicity stars. Given the generally fainter luminosities of our AGN sample, a natural follow up study would be to include brighter AGN with more robust LyC detections outside the UVCANDELS fields, such as those in Grazian et al. (2018) and Romano et al. (2019), which could potentially result in more accurate correlation fits.

## 8. CONCLUSIONS

We measured the escaping LyC flux from 51 AGN with high quality spectroscopic redshifts found in the UVCANDELS, ERS, HDUV, and UVUDF data after an exhaustive search of Vizier AGN databases. We found 12 AGN with LyC emission where the detection reached a  $\text{SNR} > 4\sigma$ . We used best-fitting CIGALE SEDs to model all of our AGN intrinsic flux and physical parameters using the highest SNR photometric data retrieved from NED database queries, ranging from X-ray to radio. We used these models, along with the IGM MC code of Inoue et al. (2014), to calculate the  $f_{\text{esc}}$  of the 12 AGN with LyC detections. We correlated the SED parameters with the LyC flux of our AGN and fit lines to these correlations using a Bayesian regression, treating non-detections as censored data. We also stacked LyC cutout images of subsamples of AGN based on detected regions in the electromagnetic spectrum using the NED photometry, as well as subsamples of AGN based on the proximity of their LyC filter cutoff to their observed-frame Lyman-limit. Our results are as follows:

- (1) The CIGALE SED fits of our 51 AGN indicate a weak, dusty, and mildly star-forming AGN population. From KS-tests, the 12 LyC-detected AGN are not distinguishable from the non-LyC-detected AGN in SED parameter histograms. The LyC-detected AGN  $f_{\text{esc}}$  values show a wide range, from  $1\% \lesssim f_{\text{esc}} \lesssim 100\%$ , or more (indicative of observed LyC

flux outshining model predictions), with an inverse-variance weighted-average  $f_{\text{esc}} \simeq 18\%$ .

(2) We find no significant correlations of the LyC emission for the stacked subsamples based on their detections in the various regions of the AGN continuum. The brightest substack in LyC was the sub-mm stack in F336W ( $3.15 < z < 3.71$ ), although this stack had three AGN and likely has a detection bias. The full stack of all 51 AGN was the brightest stack compared to stacks of all AGN detected in some region of the AGN continuum. The stack of all galaxies in the F336W sample ( $3.08 < z < 4.88$  ( $z \sim 3.5924$ ) containing 16 AGN was the brightest substack with  $m_{\text{AB}} = 27.66 \pm 0.56$ , outshining the two lower redshift bins at  $2.28 < z < 2.30$  and  $2.38 < z < 3.08$ . After splitting each of these three samples by their median redshift into higher and lower redshift bins, then stacking these subsamples, we find that the lower- $z$  substacks show brighter LyC flux.

(3) On an individual basis, we find significant correlation between the observed LyC flux and the 2–10 keV X-ray luminosity, the main stellar population’s star-formation onset age, AGN disk luminosity, AGN torus luminosity, the AGN monochromatic  $6 \mu\text{m}$  luminosity, and the AGN 1.4 GHz power. We also find significant anti-correlation of the measured LyC flux with stellar metallicity and  $A_{FUV}$ . These findings indicate a connection to the emitted LyC flux and X-ray and thermal dust emission, and indicate that more recent star-formation episodes produce higher LyC emission, where LyC emission also favors metal poor galaxies.

Although these correlations may not be exactly linear in nature, they do suggest a monotonically increasing relationship to observed LyC flux. The result of only finding 12 detections out of 51 AGN, with no evidence for redshift dependence, shows that the physical environments of the AGN and host-galaxy must play an intimate role in the escape of LyC. Our sample of AGN is still small, and only covers a redshift range from  $z \sim 2.3$ –4.9. However, we are beginning to ascertain the physical origins for LyC escape in AGN with

this small sample. This analysis should be expanded upon, both with more HST WFC3/UVIS data and to lower redshift using data from higher energy observatories. Expanding the sample to higher redshifts may be challenging given the increasing opacity of the IGM. Since AGN show essentially no evolution in their SED over cosmic time, the correlation of their physical parameters to their LyC emission could reveal the true impact of AGN on reionization. Their inferred LyC flux at the most relevant redshifts at  $z \geq 6$  could ideally be obtained simply by finding where these high- $z$  AGN lie on some correlated curves of LyC flux vs. a measurable physical parameter.

<sup>1</sup> We thank A. Inoue for providing the essential IGM attenuation montecarlo code used for  $f_{\text{esc}}$  calculations. This work is  
<sup>2</sup> based on observations with the NASA/ESA Hubble Space  
<sup>3</sup> Telescope obtained at the Space Telescope Science Institute,  
<sup>4</sup> which is operated by the Association of Universities  
<sup>5</sup> for Research in Astronomy, Incorporated, under NASA con-  
<sup>6</sup> tract NAS5-26555. Support for Program number HST-GO-  
<sup>7</sup> 15647 was provided through a grant from the STScI under  
<sup>8</sup> NASA contract NAS5-26555. RAW acknowledges support  
<sup>9</sup> from NASA JWST Interdisciplinary Scientist grants NAG5-  
<sup>10</sup> 12460, NNX14AN10G and 80NSSC18K0200 from GSFC.  
<sup>11</sup> XW acknowledges work carried out, in part, by IPAC at the  
<sup>12</sup> California Institute of Technology, and was sponsored by the  
<sup>13</sup> National Aeronautics and Space Administration. XW is sup-  
<sup>14</sup> ported by the Fundamental Research Funds for the Central  
<sup>15</sup> Universities, and the CAS Project for Young Scientists in Ba-  
<sup>16</sup> sic Research, Grant No. YSBR-062. This research has made  
<sup>17</sup> use of the NASA/IPAC Extragalactic Database (NED), which  
<sup>18</sup> is funded by the National Aeronautics and Space Administra-  
<sup>19</sup> tion and operated by the California Institute of Technology.

### Facilities: HST(ACS, WFC3)

**Software:** astropy (Astropy Collaboration et al. 2013, 2018, 2022), CIGALE (Boquien et al. 2019), SExtractor (Bertin & Arnouts 1996)

## REFERENCES

- Abazajian, K., Adelman-McCarthy, J. K., Agüeros, M. A., et al. 2004, AJ, 128, 502, doi: [10.1086/421365](https://doi.org/10.1086/421365)
- Adelman-McCarthy, J. K., Agüeros, M. A., Allam, S. S., et al. 2008, The Astrophysical Journal Supplement Series, 175, 297, doi: [10.1086/524984](https://doi.org/10.1086/524984)
- Afonso, J., Mobasher, B., Koekemoer, A., Norris, R. P., & Cram, L. 2006, AJ, 131, 1216, doi: [10.1086/498823](https://doi.org/10.1086/498823)
- Aghanim, N., Akrami, Y., Ashdown, M., et al. 2020, A&A, 641, A6, doi: [10.1051/0004-6361/201833910](https://doi.org/10.1051/0004-6361/201833910)
- Aird, J., Nandra, K., Georgakakis, A., et al. 2008, MNRAS, 387, 883, doi: [10.1111/j.1365-2966.2008.13286.x](https://doi.org/10.1111/j.1365-2966.2008.13286.x)
- Akiyama, M. 2005, ApJ, 629, 72, doi: [10.1086/431291](https://doi.org/10.1086/431291)
- Albareti, F. D., Allende Prieto, C., Almeida, A., et al. 2017, ApJS, 233, 25, doi: [10.3847/1538-4365/aa8992](https://doi.org/10.3847/1538-4365/aa8992)
- Alexander, D. M., Bauer, F. E., Brandt, W. N., et al. 2003, AJ, 126, 539, doi: [10.1086/376473](https://doi.org/10.1086/376473)
- Alonso-Herrero, A., Pérez-González, P. G., Alexander, D. M., et al. 2006, ApJ, 640, 167, doi: [10.1086/499800](https://doi.org/10.1086/499800)
- Antonucci, M., Talavera, A., Vagnetti, F., et al. 2015, A&A, 574, A49, doi: [10.1051/0004-6361/201425010](https://doi.org/10.1051/0004-6361/201425010)
- Ashby, M. L. N., Willner, S. P., Fazio, G. G., et al. 2015, ApJS, 218, 33, doi: [10.1088/0067-0049/218/2/33](https://doi.org/10.1088/0067-0049/218/2/33)
- Ashcraft, T. A., Windhorst, R. A., Jansen, R. A., et al. 2018, PASP, 130, 064102, doi: [10.1088/1538-3873/aab542](https://doi.org/10.1088/1538-3873/aab542)

- Ashcraft, T. A., McCabe, T., Redshaw, C., et al. 2023, PASP, 135, 024101, doi: [10.1088/1538-3873/aca1e0](https://doi.org/10.1088/1538-3873/aca1e0)
- Astropy Collaboration, Robitaille, T. P., Tollerud, E. J., et al. 2013, A&A, 558, A33, doi: [10.1051/0004-6361/201322068](https://doi.org/10.1051/0004-6361/201322068)
- Astropy Collaboration, Price-Whelan, A. M., Sipőcz, B. M., et al. 2018, AJ, 156, 123, doi: [10.3847/1538-3881/aabc4f](https://doi.org/10.3847/1538-3881/aabc4f)
- Astropy Collaboration, Price-Whelan, A. M., Lim, P. L., et al. 2022, ApJ, 935, 167, doi: [10.3847/1538-4357/ac7c74](https://doi.org/10.3847/1538-4357/ac7c74)
- Bañados, E., Venemans, B. P., Mazzucchelli, C., et al. 2018, Nature, 553, 473, doi: [10.1038/nature25180](https://doi.org/10.1038/nature25180)
- Balestra, I., Mainieri, V., Popesso, P., et al. 2010, A&A, 512, A12, doi: [10.1051/0004-6361/200913626](https://doi.org/10.1051/0004-6361/200913626)
- Barger, A. J., Cowie, L. L., & Wang, W. H. 2008, ApJ, 689, 687, doi: [10.1086/592735](https://doi.org/10.1086/592735)
- Barger, A. J., Cowie, L. L., Capak, P., et al. 2003, AJ, 126, 632, doi: [10.1086/376843](https://doi.org/10.1086/376843)
- Barth, A. J., Martini, P., Nelson, C. H., & Ho, L. C. 2003, ApJL, 594, L95, doi: [10.1086/378735](https://doi.org/10.1086/378735)
- Becker, R. H., Fan, X., White, R. L., et al. 2001, AJ, 122, 2850, doi: [10.1086/324231](https://doi.org/10.1086/324231)
- Beckwith, S. V. W., Stiavelli, M., Koekemoer, A. M., et al. 2006, AJ, 132, 1729, doi: [10.1086/507302](https://doi.org/10.1086/507302)
- Bertin, E., & Arnouts, S. 1996, A&AS, 117, 393, doi: [10.1051/aas:1996164](https://doi.org/10.1051/aas:1996164)
- Biggs, A. D., & Ivison, R. J. 2006, MNRAS, 371, 963, doi: [10.1111/j.1365-2966.2006.10730.x](https://doi.org/10.1111/j.1365-2966.2006.10730.x)
- Bizzocchi, L., Filho, M. E., Leonardo, E., et al. 2014, ApJ, 782, 22, doi: [10.1088/0004-637X/782/1/22](https://doi.org/10.1088/0004-637X/782/1/22)
- Bolan, P., Lemaux, B. C., Mason, C., et al. 2022, MNRAS, 517, 3263, doi: [10.1093/mnras/stac1963](https://doi.org/10.1093/mnras/stac1963)
- Boquien, M., Burgarella, D., Roehlly, Y., et al. 2019, A&A, 622, A103, doi: [10.1051/0004-6361/201834156](https://doi.org/10.1051/0004-6361/201834156)
- Borys, C., Smail, I., Chapman, S. C., et al. 2005, ApJ, 635, 853, doi: [10.1086/491617](https://doi.org/10.1086/491617)
- Bosman, S. E. I., Davies, F. B., Becker, G. D., et al. 2022, MNRAS, 514, 55, doi: [10.1093/mnras/stac1046](https://doi.org/10.1093/mnras/stac1046)
- Bouwens, R. J., Illingworth, G. D., Oesch, P. A., et al. 2015, ApJ, 811, 140, doi: [10.1088/0004-637X/811/2/140](https://doi.org/10.1088/0004-637X/811/2/140)
- Bouwens, R. J., Illingworth, G. D., Thompson, R. I., & Franx, M. 2005, ApJL, 624, L5, doi: [10.1086/430302](https://doi.org/10.1086/430302)
- Bouwens, R. J., Illingworth, G. D., Oesch, P. A., et al. 2014, ApJ, 793, 115, doi: [10.1088/0004-637X/793/2/115](https://doi.org/10.1088/0004-637X/793/2/115)
- Brandt, W. N., Alexander, D. M., Hornschemeier, A. E., et al. 2001, The Astronomical Journal, 122, 2810, doi: [10.1086/324105](https://doi.org/10.1086/324105)
- Brightman, M., Nandra, K., Salvato, M., et al. 2014, MNRAS, 443, 1999, doi: [10.1093/mnras/stu1175](https://doi.org/10.1093/mnras/stu1175)
- Bruzual, G., & Charlot, S. 2003, MNRAS, 344, 1000, doi: [10.1046/j.1365-8711.2003.06897.x](https://doi.org/10.1046/j.1365-8711.2003.06897.x)
- Buchner, J., Georgakakis, A., Nandra, K., et al. 2014, A&A, 564, A125, doi: [10.1051/0004-6361/201322971](https://doi.org/10.1051/0004-6361/201322971)
- Cameron, E., Carollo, C. M., Oesch, P. A., et al. 2011, ApJ, 743, 146, doi: [10.1088/0004-637X/743/2/146](https://doi.org/10.1088/0004-637X/743/2/146)
- Cappelluti, N., Comastri, A., Fontana, A., et al. 2016, ApJ, 823, 95, doi: [10.3847/0004-637X/823/2/95](https://doi.org/10.3847/0004-637X/823/2/95)
- Cardamone, C. N., Urry, C. M., Damen, M., et al. 2008, ApJ, 680, 130, doi: [10.1086/587800](https://doi.org/10.1086/587800)
- Carilli, C. L., Daddi, E., Riechers, D., et al. 2010, ApJ, 714, 1407, doi: [10.1088/0004-637X/714/2/1407](https://doi.org/10.1088/0004-637X/714/2/1407)
- Chen, H.-W., & Marzke, R. O. 2004, ApJ, 615, 603, doi: [10.1086/424732](https://doi.org/10.1086/424732)
- Chen, P. S., & Shan, H. G. 2009, MNRAS, 393, 1408, doi: [10.1111/j.1365-2966.2008.14222.x](https://doi.org/10.1111/j.1365-2966.2008.14222.x)
- Ciesla, L., Elbaz, D., & Fensch, J. 2017, A&A, 608, A41, doi: [10.1051/0004-6361/201731036](https://doi.org/10.1051/0004-6361/201731036)
- Coe, D., Benítez, N., Sánchez, S. F., et al. 2006, AJ, 132, 926, doi: [10.1086/505530](https://doi.org/10.1086/505530)
- Cowie, L. L., Barger, A. J., Fomalont, E. B., & Capak, P. 2004, ApJL, 603, L69, doi: [10.1086/383198](https://doi.org/10.1086/383198)
- Cowie, L. L., Barger, A. J., Hsu, L. Y., et al. 2017, ApJ, 837, 139, doi: [10.3847/1538-4357/aa60bb](https://doi.org/10.3847/1538-4357/aa60bb)
- Cutri, R. M., Wright, E. L., Conrow, T., et al. 2013, Explanatory Supplement to the AllWISE Data Release Products, Explanatory Supplement to the AllWISE Data Release Products, by R. M. Cutri et al.
- . 2014, VizieR Online Data Catalog, II/328
- Daddi, E., Dannerbauer, H., Stern, D., et al. 2009, ApJ, 694, 1517, doi: [10.1088/0004-637X/694/2/1517](https://doi.org/10.1088/0004-637X/694/2/1517)
- Del Moro, A., Alexander, D. M., Bauer, F. E., et al. 2016, MNRAS, 456, 2105, doi: [10.1093/mnras/stv2748](https://doi.org/10.1093/mnras/stv2748)
- Djorgovski, S. G., Castro, S., Stern, D., & Mahabal, A. A. 2001, ApJL, 560, L5, doi: [10.1086/324175](https://doi.org/10.1086/324175)
- Donley, J. L., Rieke, G. H., Pérez-González, P. G., Rigby, J. R., & Alonso-Herrero, A. 2007, ApJ, 660, 167, doi: [10.1086/512798](https://doi.org/10.1086/512798)
- Falocco, S., Paolillo, M., Covone, G., et al. 2015, A&A, 579, A115, doi: [10.1051/0004-6361/201425111](https://doi.org/10.1051/0004-6361/201425111)
- Fan, X., Hennawi, J. F., Richards, G. T., et al. 2004, AJ, 128, 515, doi: [10.1086/422434](https://doi.org/10.1086/422434)
- Fan, X., Strauss, M. A., Becker, R. H., et al. 2006, AJ, 132, 117, doi: [10.1086/504836](https://doi.org/10.1086/504836)
- Ferland, G. J., Korista, K. T., Verner, D. A., et al. 1998, PASP, 110, 761, doi: [10.1086/316190](https://doi.org/10.1086/316190)
- Ferland, G. J., Porter, R. L., van Hoof, P. A. M., et al. 2013, RMxAA, 49, 137, doi: [10.48550/arXiv.1302.4485](https://doi.org/10.48550/arXiv.1302.4485)
- Finkelstein, S. L., Rhoads, J. E., Malhotra, S., Grogin, N., & Wang, J. 2008, ApJ, 678, 655, doi: [10.1086/525272](https://doi.org/10.1086/525272)
- Finkelstein, S. L., D’Aloisio, A., Paardekooper, J.-P., et al. 2019, ApJ, 879, 36, doi: [10.3847/1538-4357/ab1ea8](https://doi.org/10.3847/1538-4357/ab1ea8)
- Finkelstein, S. L., Bagley, M. B., Haro, P. A., et al. 2022, ApJL, 940, L55, doi: [10.3847/2041-8213/ac966e](https://doi.org/10.3847/2041-8213/ac966e)

- Flury, S. R., Jaskot, A. E., Ferguson, H. C., et al. 2022, ApJS, 260, 1, doi: [10.3847/1538-4365/ac5331](https://doi.org/10.3847/1538-4365/ac5331)
- Fontanot, F., Cristiani, S., Grazian, A., et al. 2023, MNRAS, 520, 740, doi: [10.1093/mnras/stad189](https://doi.org/10.1093/mnras/stad189)
- Franzen, T. M. O., Banfield, J. K., Hales, C. A., et al. 2015, MNRAS, 453, 4020, doi: [10.1093/mnras/stv1866](https://doi.org/10.1093/mnras/stv1866)
- Garilli, B., McLure, R., Pentericci, L., et al. 2021, A&A, 647, A150, doi: [10.1051/0004-6361/202040059](https://doi.org/10.1051/0004-6361/202040059)
- Gattano, C., Souchay, J., & Barache, C. 2014, A&A, 564, A117, doi: [10.1051/0004-6361/201323238](https://doi.org/10.1051/0004-6361/201323238)
- Georgantopoulos, I., Rovilos, E., Xilouris, E. M., Comastri, A., & Akylas, A. 2011, A&A, 526, A86, doi: [10.1051/0004-6361/201014417](https://doi.org/10.1051/0004-6361/201014417)
- Giallongo, E., Grazian, A., Fiore, F., et al. 2015, A&A, 578, A83, doi: [10.1051/0004-6361/201425334](https://doi.org/10.1051/0004-6361/201425334)
- . 2019, ApJ, 884, 19, doi: [10.3847/1538-4357/ab39e1](https://doi.org/10.3847/1538-4357/ab39e1)
- Giménez-Arteaga, C., Oesch, P. A., Brammer, G. B., et al. 2023, ApJ, 948, 126, doi: [10.3847/1538-4357/acc5ea](https://doi.org/10.3847/1538-4357/acc5ea)
- Goto, T., Utsumi, Y., Hattori, T., Miyazaki, S., & Yamauchi, C. 2011, MNRAS, 415, L1, doi: [10.1111/j.1745-3933.2011.01063.x](https://doi.org/10.1111/j.1745-3933.2011.01063.x)
- Grazian, A., Giallongo, E., Boutsia, K., et al. 2018, A&A, 613, A44, doi: [10.1051/0004-6361/201732385](https://doi.org/10.1051/0004-6361/201732385)
- Grazian, A., Giallongo, E., Fiore, F., et al. 2020, ApJ, 897, 94, doi: [10.3847/1538-4357/ab99a3](https://doi.org/10.3847/1538-4357/ab99a3)
- Grazian, A., Giallongo, E., Boutsia, K., et al. 2022, ApJ, 924, 62, doi: [10.3847/1538-4357/ac33a4](https://doi.org/10.3847/1538-4357/ac33a4)
- Griffiths, A., Conselice, C. J., Ferreira, L., et al. 2022, ApJ, 941, 181, doi: [10.3847/1538-4357/aca296](https://doi.org/10.3847/1538-4357/aca296)
- Guidetti, D., Bondi, M., Prandoni, I., et al. 2017, MNRAS, 471, 210, doi: [10.1093/mnras/stx1162](https://doi.org/10.1093/mnras/stx1162)
- Haardt, F., & Maraschi, L. 1991, ApJL, 380, L51, doi: [10.1086/186171](https://doi.org/10.1086/186171)
- Harikane, Y., Ouchi, M., Ono, Y., et al. 2016, ApJ, 821, 123, doi: [10.3847/0004-637X/821/2/123](https://doi.org/10.3847/0004-637X/821/2/123)
- Hashimoto, T., Laporte, N., Mawatari, K., et al. 2018, Nature, 557, 392, doi: [10.1038/s41586-018-0117-z](https://doi.org/10.1038/s41586-018-0117-z)
- Herenz, E. C., Urrutia, T., Wisotzki, L., et al. 2017, A&A, 606, A12, doi: [10.1051/0004-6361/201731055](https://doi.org/10.1051/0004-6361/201731055)
- Hodge, J. A., Carilli, C. L., Walter, F., et al. 2012, ApJ, 760, 11, doi: [10.1088/0004-637X/760/1/11](https://doi.org/10.1088/0004-637X/760/1/11)
- Hsu, L.-T., Salvato, M., Nandra, K., et al. 2014, ApJ, 796, 60, doi: [10.1088/0004-637X/796/1/60](https://doi.org/10.1088/0004-637X/796/1/60)
- Huang, J. S., Rigopoulou, D., Magdis, G., et al. 2014, ApJ, 784, 52, doi: [10.1088/0004-637X/784/1/52](https://doi.org/10.1088/0004-637X/784/1/52)
- Huynh, M. T., Bell, M. E., Hopkins, A. M., Norris, R. P., & Seymour, N. 2015, MNRAS, 454, 952, doi: [10.1093/mnras/stv2012](https://doi.org/10.1093/mnras/stv2012)
- Inami, H., Bacon, R., Brinchmann, J., et al. 2017, A&A, 608, A2, doi: [10.1051/0004-6361/201731195](https://doi.org/10.1051/0004-6361/201731195)
- Inoue, A. K., Shimizu, I., Iwata, I., & Tanaka, M. 2014, MNRAS, 442, 1805, doi: [10.1093/mnras/stu936](https://doi.org/10.1093/mnras/stu936)
- Iwamuro, F., Kimura, M., Eto, S., et al. 2004, ApJ, 614, 69, doi: [10.1086/423610](https://doi.org/10.1086/423610)
- Izotov, Y. I., Worseck, G., Schaerer, D., et al. 2021, MNRAS, 503, 1734, doi: [10.1093/mnras/stab612](https://doi.org/10.1093/mnras/stab612)
- Jahnke, K., Sánchez, S. F., Wisotzki, L., et al. 2004, ApJ, 614, 568, doi: [10.1086/423233](https://doi.org/10.1086/423233)
- Jiang, L., Fan, X., Vestergaard, M., et al. 2007, AJ, 134, 1150, doi: [10.1086/520811](https://doi.org/10.1086/520811)
- Jiménez-Teja, Y., Benítez, N., Molino, A., & Fernandes, C. A. C. 2015, MNRAS, 453, 1136, doi: [10.1093/mnras/stv1612](https://doi.org/10.1093/mnras/stv1612)
- Kellermann, K. I., Fomalont, E. B., Mainieri, V., et al. 2008, ApJS, 179, 71, doi: [10.1086/591055](https://doi.org/10.1086/591055)
- Kelly, B. C., Bechtold, J., Siemiginowska, A., Aldcroft, T., & Sobolewska, M. 2007, ApJ, 657, 116, doi: [10.1086/510876](https://doi.org/10.1086/510876)
- Khaire, V., Srianand, R., Choudhury, T. R., & Gaikwad, P. 2016, MNRAS, 457, 4051, doi: [10.1093/mnras/stw192](https://doi.org/10.1093/mnras/stw192)
- Kim, Y., Im, M., Jeon, Y., et al. 2020, ApJ, 904, 111, doi: [10.3847/1538-4357/abc0ea](https://doi.org/10.3847/1538-4357/abc0ea)
- Kirkpatrick, A., Pope, A., Alexander, D. M., et al. 2012, ApJ, 759, 139, doi: [10.1088/0004-637X/759/2/139](https://doi.org/10.1088/0004-637X/759/2/139)
- Koekemoer, A. M., Alexander, D. M., Bauer, F. E., et al. 2004, ApJL, 600, L123, doi: [10.1086/378181](https://doi.org/10.1086/378181)
- Kovács, A., Chapman, S. C., Dowell, C. D., et al. 2006, ApJ, 650, 592, doi: [10.1086/506341](https://doi.org/10.1086/506341)
- Kulkarni, G., Worseck, G., & Hennawi, J. F. 2019, MNRAS, 488, 1035, doi: [10.1093/mnras/stz1493](https://doi.org/10.1093/mnras/stz1493)
- Kurk, J., Cimatti, A., Daddi, E., et al. 2013, A&A, 549, A63, doi: [10.1051/0004-6361/201117847](https://doi.org/10.1051/0004-6361/201117847)
- Laird, E. S., Nandra, K., Hobbs, A., & Steidel, C. C. 2006, MNRAS, 373, 217, doi: [10.1111/j.1365-2966.2006.11002.x](https://doi.org/10.1111/j.1365-2966.2006.11002.x)
- Laporte, N., Meyer, R. A., Ellis, R. S., et al. 2021, MNRAS, 505, 3336, doi: [10.1093/mnras/stab1239](https://doi.org/10.1093/mnras/stab1239)
- Le Fèvre, O., Vettolani, G., Paltani, S., et al. 2004, A&A, 428, 1043, doi: [10.1051/0004-6361:20048072](https://doi.org/10.1051/0004-6361:20048072)
- Leitherer, C., Hernandez, S., Lee, J. C., & Oey, M. S. 2016, ApJ, 823, 64, doi: [10.3847/0004-637X/823/1/64](https://doi.org/10.3847/0004-637X/823/1/64)
- Liu, D., Daddi, E., Dickinson, M., et al. 2018, ApJ, 853, 172, doi: [10.3847/1538-4357/aaa600](https://doi.org/10.3847/1538-4357/aaa600)
- Luo, B., Brandt, W. N., Xue, Y. Q., et al. 2017, ApJS, 228, 2, doi: [10.3847/1538-4365/228/1/2](https://doi.org/10.3847/1538-4365/228/1/2)
- Lusso, E., Worseck, G., Hennawi, J. F., et al. 2015, Monthly Notices of the Royal Astronomical Society, 449, 4204, doi: [10.1093/mnras/stv516](https://doi.org/10.1093/mnras/stv516)
- Lutz, D., Mainieri, V., Rafferty, D., et al. 2010, ApJ, 712, 1287, doi: [10.1088/0004-637X/712/2/1287](https://doi.org/10.1088/0004-637X/712/2/1287)
- Madau, P., & Haardt, F. 2015, ApJL, 813, L8, doi: [10.1088/2041-8205/813/1/L8](https://doi.org/10.1088/2041-8205/813/1/L8)

- Magnelli, B., Elbaz, D., Chary, R. R., et al. 2011, *A&A*, 528, A35, doi: [10.1051/0004-6361/200913941](https://doi.org/10.1051/0004-6361/200913941)
- Mainieri, V., Kellermann, K. I., Fomalont, E. B., et al. 2008, *ApJS*, 179, 95, doi: [10.1086/591053](https://doi.org/10.1086/591053)
- Mancini, C., Matute, I., Cimatti, A., et al. 2009, *A&A*, 500, 705, doi: [10.1051/0004-6361/200810630](https://doi.org/10.1051/0004-6361/200810630)
- Marchi, F., Pentericci, L., Guaita, L., et al. 2018, *A&A*, 614, A11, doi: [10.1051/0004-6361/201732133](https://doi.org/10.1051/0004-6361/201732133)
- Matsuoka, Y., Onoue, M., Kashikawa, N., et al. 2019, *ApJL*, 872, L2, doi: [10.3847/2041-8213/ab0216](https://doi.org/10.3847/2041-8213/ab0216)
- McGreer, I. D., Fan, X., Jiang, L., & Cai, Z. 2018, *AJ*, 155, 131, doi: [10.3847/1538-3881/aaaab4](https://doi.org/10.3847/1538-3881/aaaab4)
- Miller, N. A., Fomalont, E. B., Kellermann, K. I., et al. 2008, *ApJS*, 179, 114, doi: [10.1086/591054](https://doi.org/10.1086/591054)
- Morrison, G. E., Owen, F. N., Dickinson, M., Ivison, R. J., & Ibar, E. 2010, *ApJS*, 188, 178, doi: [10.1088/0067-0049/188/1/178](https://doi.org/10.1088/0067-0049/188/1/178)
- Mortlock, D. J., Warren, S. J., Venemans, B. P., et al. 2011, *Nature*, 474, 616, doi: [10.1038/nature10159](https://doi.org/10.1038/nature10159)
- Mutch, S. J., Greig, B., Qin, Y., Poole, G. B., & Wyithe, J. S. B. 2023, arXiv e-prints, arXiv:2303.07378, doi: [10.48550/arXiv.2303.07378](https://doi.org/10.48550/arXiv.2303.07378)
- Negrello, M., Serjeant, S., Pearson, C., et al. 2009, *MNRAS*, 394, 375, doi: [10.1111/j.1365-2966.2008.14293.x](https://doi.org/10.1111/j.1365-2966.2008.14293.x)
- Niida, M., Nagao, T., Ikeda, H., et al. 2020, *ApJ*, 904, 89, doi: [10.3847/1538-4357/abbe11](https://doi.org/10.3847/1538-4357/abbe11)
- O'Brien, R., Carleton, T., Windhorst, R. A., et al. 2023, *AJ*, 165, 237, doi: [10.3847/1538-3881/accee](https://doi.org/10.3847/1538-3881/accee)
- Ochsenbein, F., Bauer, P., & Marcout, J. 2000, *A&AS*, 143, 23, doi: [10.1051/aas:2000169](https://doi.org/10.1051/aas:2000169)
- Oesch, P. A., Montes, M., Reddy, N., et al. 2018, *The Astrophysical Journal Supplement Series*, 237, 12, doi: [10.3847/1538-4365/aacb30](https://doi.org/10.3847/1538-4365/aacb30)
- Oke, J. B., & Gunn, J. E. 1983, *ApJ*, 266, 713, doi: [10.1086/160817](https://doi.org/10.1086/160817)
- Onoue, M., Inayoshi, K., Ding, X., et al. 2023, *ApJL*, 942, L17, doi: [10.3847/2041-8213/aca9d3](https://doi.org/10.3847/2041-8213/aca9d3)
- Otteson, L., McCabe, T., Ashcraft, T. A., et al. 2021, *Research Notes of the American Astronomical Society*, 5, 190, doi: [10.3847/2515-5172/ac1db6](https://doi.org/10.3847/2515-5172/ac1db6)
- Pahl, A. J., Shapley, A., Steidel, C. C., Chen, Y., & Reddy, N. A. 2021, *MNRAS*, 505, 2447, doi: [10.1093/mnras/stab1374](https://doi.org/10.1093/mnras/stab1374)
- Parsa, S., Dunlop, J. S., & McLure, R. J. 2018, *MNRAS*, 474, 2904, doi: [10.1093/mnras/stx2887](https://doi.org/10.1093/mnras/stx2887)
- Pearson, C. P., Serjeant, S., Negrello, M., et al. 2010, *A&A*, 514, A9, doi: [10.1051/0004-6361/200913383](https://doi.org/10.1051/0004-6361/200913383)
- Penner, K., Pope, A., Chapin, E. L., et al. 2011, *MNRAS*, 410, 2749, doi: [10.1111/j.1365-2966.2010.17650.x](https://doi.org/10.1111/j.1365-2966.2010.17650.x)
- Petrucci, P. O., Gronkiewicz, D., Rozanska, A., et al. 2020, *A&A*, 634, A85, doi: [10.1051/0004-6361/201937011](https://doi.org/10.1051/0004-6361/201937011)
- Pope, A., Borys, C., Scott, D., et al. 2005, *MNRAS*, 358, 149, doi: [10.1111/j.1365-2966.2005.08759.x](https://doi.org/10.1111/j.1365-2966.2005.08759.x)
- Popesso, P., Dickinson, M., Nonino, M., et al. 2009, *A&A*, 494, 443, doi: [10.1051/0004-6361:200809617](https://doi.org/10.1051/0004-6361:200809617)
- Puccetti, S., Capalbi, M., Giommi, P., et al. 2011, *A&A*, 528, A122, doi: [10.1051/0004-6361/201015560](https://doi.org/10.1051/0004-6361/201015560)
- Qin, Y., Mesinger, A., Bosman, S. E. I., & Viel, M. 2021, *MNRAS*, 506, 2390, doi: [10.1093/mnras/stab1833](https://doi.org/10.1093/mnras/stab1833)
- Rafelski, M., Teplitz, H. I., Gardner, J. P., et al. 2015, *AJ*, 150, 31, doi: [10.1088/0004-6256/150/1/31](https://doi.org/10.1088/0004-6256/150/1/31)
- Reddy, N. A., & Steidel, C. C. 2009, *ApJ*, 692, 778, doi: [10.1088/0004-637X/692/1/778](https://doi.org/10.1088/0004-637X/692/1/778)
- Reddy, N. A., Steidel, C. C., Erb, D. K., Shapley, A. E., & Pettini, M. 2006, *ApJ*, 653, 1004, doi: [10.1086/508851](https://doi.org/10.1086/508851)
- Redshaw, C., McCabe, T., Otteson, L., et al. 2022, *Research Notes of the American Astronomical Society*, 6, 63, doi: [10.3847/2515-5172/ac6189](https://doi.org/10.3847/2515-5172/ac6189)
- Reis, R. C., Miller, J. M., Fabian, A. C., et al. 2011, *MNRAS*, 410, 2497, doi: [10.1111/j.1365-2966.2010.17628.x](https://doi.org/10.1111/j.1365-2966.2010.17628.x)
- Rigby, J. R., Rieke, G. H., Pérez-González, P. G., et al. 2005, *ApJ*, 627, 134, doi: [10.1086/430398](https://doi.org/10.1086/430398)
- Rigopoulou, D., Mainieri, V., Almaini, O., et al. 2009, *MNRAS*, 400, 1199, doi: [10.1111/j.1365-2966.2009.15543.x](https://doi.org/10.1111/j.1365-2966.2009.15543.x)
- Robertson, B. E., Tacchella, S., Johnson, B. D., et al. 2023, *Nature Astronomy*, 7, 611, doi: [10.1038/s41550-023-01921-1](https://doi.org/10.1038/s41550-023-01921-1)
- Rodighiero, G., Cimatti, A., Franceschini, A., et al. 2007, *A&A*, 470, 21, doi: [10.1051/0004-6361:20066497](https://doi.org/10.1051/0004-6361:20066497)
- Romano, M., Grazian, A., Giallongo, E., et al. 2019, *A&A*, 632, A45, doi: [10.1051/0004-6361/201935550](https://doi.org/10.1051/0004-6361/201935550)
- Rosen, S. R., Webb, N. A., Watson, M. G., et al. 2016, *A&A*, 590, A1, doi: [10.1051/0004-6361/201526416](https://doi.org/10.1051/0004-6361/201526416)
- Rutkowski, M. J., Scarlata, C., Henry, A., et al. 2017, *ApJL*, 841, L27, doi: [10.3847/2041-8213/aa733b](https://doi.org/10.3847/2041-8213/aa733b)
- Saldana-Lopez, A., Schaefer, D., Chisholm, J., et al. 2023, *MNRAS*, 522, 6295, doi: [10.1093/mnras/stad1283](https://doi.org/10.1093/mnras/stad1283)
- Shen, Y., Wu, J., Jiang, L., et al. 2019, *ApJ*, 873, 35, doi: [10.3847/1538-4357/ab03d9](https://doi.org/10.3847/1538-4357/ab03d9)
- Shim, H., Chary, R.-R., Dickinson, M., et al. 2011, *ApJ*, 738, 69, doi: [10.1088/0004-637X/738/1/69](https://doi.org/10.1088/0004-637X/738/1/69)
- Skelton, R. E., Whitaker, K. E., Momcheva, I. G., et al. 2014, *ApJS*, 214, 24, doi: [10.1088/0067-0049/214/2/24](https://doi.org/10.1088/0067-0049/214/2/24)
- Smail, I., Chapman, S. C., Blain, A. W., & Ivison, R. J. 2004, *ApJ*, 616, 71, doi: [10.1086/424896](https://doi.org/10.1086/424896)
- Smith, B. M., Windhorst, R. A., Jansen, R. A., et al. 2018, *ApJ*, 853, 191, doi: [10.3847/1538-4357/aaa3dc](https://doi.org/10.3847/1538-4357/aaa3dc)
- Smith, B. M., Windhorst, R. A., Cohen, S. H., et al. 2020, *ApJ*, 897, 41, doi: [10.3847/1538-4357/ab8811](https://doi.org/10.3847/1538-4357/ab8811)
- Souchay, J., Andrei, A. H., Barache, C., et al. 2012, *A&A*, 537, A99, doi: [10.1051/0004-6361/201117954](https://doi.org/10.1051/0004-6361/201117954)
- . 2015, *A&A*, 583, A75, doi: [10.1051/0004-6361/201526092](https://doi.org/10.1051/0004-6361/201526092)
- Stalevski, M., Fritz, J., Baes, M., Nakos, T., & Popović, L. Č. 2012, *MNRAS*, 420, 2756, doi: [10.1111/j.1365-2966.2011.19775.x](https://doi.org/10.1111/j.1365-2966.2011.19775.x)

- Stalevski, M., Ricci, C., Ueda, Y., et al. 2016, MNRAS, 458, 2288, doi: [10.1093/mnras/stw444](https://doi.org/10.1093/mnras/stw444)
- Steffen, A. T., Strateva, I., Brandt, W. N., et al. 2006, AJ, 131, 2826, doi: [10.1086/503627](https://doi.org/10.1086/503627)
- Steidel, C. C., Adelberger, K. L., Shapley, A. E., et al. 2003, ApJ, 592, 728, doi: [10.1086/375772](https://doi.org/10.1086/375772)
- Steidel, C. C., Bogosavljević, M., Shapley, A. E., et al. 2018, ApJ, 869, 123, doi: [10.3847/1538-4357/aaed28](https://doi.org/10.3847/1538-4357/aaed28)
- Straatman, C. M. S., Labbé, I., Spitler, L. R., et al. 2014, ApJL, 783, L14, doi: [10.1088/2041-8205/783/1/L14](https://doi.org/10.1088/2041-8205/783/1/L14)
- Straughn, A. N., Meurer, G. R., Pirzkal, N., et al. 2008, AJ, 135, 1624, doi: [10.1088/0004-6256/135/4/1624](https://doi.org/10.1088/0004-6256/135/4/1624)
- Szalay, A. S., Connolly, A. J., & Szokoly, G. P. 1999, AJ, 117, 68, doi: [10.1086/300689](https://doi.org/10.1086/300689)
- Szokoly, G. P., Bergeron, J., Hasinger, G., et al. 2004, ApJS, 155, 271, doi: [10.1086/424707](https://doi.org/10.1086/424707)
- Tacchella, S., Johnson, B. D., Robertson, B. E., et al. 2023, MNRAS, 522, 6236, doi: [10.1093/mnras/stad1408](https://doi.org/10.1093/mnras/stad1408)
- Tan, Q., Daddi, E., Magdis, G., et al. 2014, A&A, 569, A98, doi: [10.1051/0004-6361/201423905](https://doi.org/10.1051/0004-6361/201423905)
- Telfer, R. C., Zheng, W., Kriss, G. A., & Davidsen, A. F. 2002, ApJ, 565, 773, doi: [10.1086/324689](https://doi.org/10.1086/324689)
- Teplitz, H. 2018, Ultraviolet Imaging of the Cosmic Assembly Near-infrared Deep Extragalactic Legacy Survey Fields (UVCANDELS), HST Proposal. Cycle 26, ID. #15647
- Teplitz, H. I., Chary, R., Elbaz, D., et al. 2011, AJ, 141, 1, doi: [10.1088/0004-6256/141/1/1](https://doi.org/10.1088/0004-6256/141/1/1)
- Teplitz, H. I., Rafelski, M., Kurczynski, P., et al. 2013, AJ, 146, 159, doi: [10.1088/0004-6256/146/6/159](https://doi.org/10.1088/0004-6256/146/6/159)
- Thompson, R. I., Illingworth, G., Bouwens, R., et al. 2005, AJ, 130, 1, doi: [10.1086/430528](https://doi.org/10.1086/430528)
- Tie, S. S., Martini, P., Mudd, D., et al. 2017, AJ, 153, 107, doi: [10.3847/1538-3881/aa5b8d](https://doi.org/10.3847/1538-3881/aa5b8d)
- Treister, E., Virani, S., Gawiser, E., et al. 2009, ApJ, 693, 1713, doi: [10.1088/0004-637X/693/2/1713](https://doi.org/10.1088/0004-637X/693/2/1713)
- U, V., Hemmati, S., Darvish, B., et al. 2015, ApJ, 815, 57, doi: [10.1088/0004-637X/815/1/57](https://doi.org/10.1088/0004-637X/815/1/57)
- Vagnetti, F., Turriziani, S., & Trevese, D. 2011, A&A, 536, A84, doi: [10.1051/0004-6361/201118072](https://doi.org/10.1051/0004-6361/201118072)
- Vanzella, E., Cristiani, S., Dickinson, M., et al. 2006, A&A, 454, 423, doi: [10.1051/0004-6361:20054796](https://doi.org/10.1051/0004-6361:20054796)
- Véron-Cetty, M. P., & Véron, P. 2006, A&A, 455, 773, doi: [10.1051/0004-6361:20065177](https://doi.org/10.1051/0004-6361:20065177)
- Vito, F., Brandt, W. N., Yang, G., et al. 2018, MNRAS, 473, 2378, doi: [10.1093/mnras/stx2486](https://doi.org/10.1093/mnras/stx2486)
- Wang, F., Yang, J., Fan, X., et al. 2018, ApJL, 869, L9, doi: [10.3847/2041-8213/aaf1d2](https://doi.org/10.3847/2041-8213/aaf1d2)
- . 2021, ApJL, 907, L1, doi: [10.3847/2041-8213/abd8c6](https://doi.org/10.3847/2041-8213/abd8c6)
- Wang, S., Liu, J., Qiu, Y., et al. 2016, ApJS, 224, 40, doi: [10.3847/0067-0049/224/2/40](https://doi.org/10.3847/0067-0049/224/2/40)
- Wang, X., Teplitz, H. I., Smith, B. M., et al. 2023, arXiv e-prints, arXiv:2308.09064, doi: [10.48550/arXiv.2308.09064](https://doi.org/10.48550/arXiv.2308.09064)
- Weiner, B. J., Willmer, C. N. A., Faber, S. M., et al. 2006, ApJ, 653, 1027, doi: [10.1086/508921](https://doi.org/10.1086/508921)
- Wiklind, T., Dickinson, M., Ferguson, H. C., et al. 2008, ApJ, 676, 781, doi: [10.1086/524919](https://doi.org/10.1086/524919)
- Windhorst, R. A., Cohen, S. H., Hathi, N. P., et al. 2011, ApJS, 193, 27, doi: [10.1088/0067-0049/193/2/27](https://doi.org/10.1088/0067-0049/193/2/27)
- Windhorst, R. A., Carleton, T., O'Brien, R., et al. 2022, AJ, 164, 141, doi: [10.3847/1538-3881/ac82af](https://doi.org/10.3847/1538-3881/ac82af)
- Wirth, G. D., Willmer, C. N. A., Amico, P., et al. 2004, AJ, 127, 3121, doi: [10.1086/420999](https://doi.org/10.1086/420999)
- Wirth, G. D., Trump, J. R., Barro, G., et al. 2015, AJ, 150, 153, doi: [10.1088/0004-6256/150/5/153](https://doi.org/10.1088/0004-6256/150/5/153)
- Wolf, C., Meisenheimer, K., Kleinheinrich, M., et al. 2004, A&A, 421, 913, doi: [10.1051/0004-6361:20040525](https://doi.org/10.1051/0004-6361:20040525)
- Wolf, C., Dye, S., Kleinheinrich, M., et al. 2001, A&A, 377, 442, doi: [10.1051/0004-6361:20011142](https://doi.org/10.1051/0004-6361:20011142)
- Wuyts, S., Labbé, I., Förster Schreiber, N. M., et al. 2008, ApJ, 682, 985, doi: [10.1086/588749](https://doi.org/10.1086/588749)
- Wuyts, S., van Dokkum, P. G., Franx, M., et al. 2009, ApJ, 706, 885, doi: [10.1088/0004-637X/706/1/885](https://doi.org/10.1088/0004-637X/706/1/885)
- Xue, Y. Q., Luo, B., Brandt, W. N., et al. 2016, ApJS, 224, 15, doi: [10.3847/0067-0049/224/2/15](https://doi.org/10.3847/0067-0049/224/2/15)
- Yang, J., Wang, F., Fan, X., et al. 2019, AJ, 157, 236, doi: [10.3847/1538-3881/ab1be1](https://doi.org/10.3847/1538-3881/ab1be1)
- . 2020, ApJL, 897, L14, doi: [10.3847/2041-8213/ab9c26](https://doi.org/10.3847/2041-8213/ab9c26)
- . 2021, ApJ, 923, 262, doi: [10.3847/1538-4357/ac2b32](https://doi.org/10.3847/1538-4357/ac2b32)
- Yoshikawa, T., Akiyama, M., Kajisawa, M., et al. 2010, ApJ, 718, 112, doi: [10.1088/0004-637X/718/1/112](https://doi.org/10.1088/0004-637X/718/1/112)
- Young, M., Elvis, M., & Risaliti, G. 2009, ApJS, 183, 17, doi: [10.1088/0067-0049/183/1/17](https://doi.org/10.1088/0067-0049/183/1/17)
- Yung, L. Y. A., Somerville, R. S., Finkelstein, S. L., et al. 2021, MNRAS, 508, 2706, doi: [10.1093/mnras/stab2761](https://doi.org/10.1093/mnras/stab2761)
- . 2020a, MNRAS, 496, 4574, doi: [10.1093/mnras/staa1800](https://doi.org/10.1093/mnras/staa1800)
- Yung, L. Y. A., Somerville, R. S., Popping, G., & Finkelstein, S. L. 2020b, MNRAS, 494, 1002, doi: [10.1093/mnras/staa714](https://doi.org/10.1093/mnras/staa714)
- Zhu, Y., Becker, G. D., Christenson, H. M., et al. 2023, arXiv e-prints, arXiv:2308.04614, doi: [10.48550/arXiv.2308.04614](https://doi.org/10.48550/arXiv.2308.04614)

## APPENDIX

**Table 3.** AGN Photometric Properties

ID	RA (1)	Dec (2)	<i>z</i> (3)	X-ray (4)	IR (5)	MIR (6)	FIR (7)	SMM (8)	Microwave (9)	Radio (10)	Radio (11)
EIS J033201.59-274327.2	53.006594	-27.724166	2.7212	31.29±0.03 <sup>5</sup>	22.53±0.01 <sup>3</sup>	21.93±0.01 <sup>1</sup>	18.82±0.03 <sup>1</sup>	...	...	...	...
CANDELS J033202.12-274327.6 <sup>†</sup>	53.008878	-27.724353	2.7226	33.54±0.08 <sup>3</sup>	24.00±0.03 <sup>1</sup>	23.38±0.02 <sup>1</sup>	20.61±0.40 <sup>1</sup>	...	...	...	...
CANDELS J033203.03-274450.0	53.01265	-27.747243	2.573	...	22.64±0.01 <sup>3</sup>	21.75±0.01 <sup>1</sup>	20.21±0.10 <sup>1</sup>	...	...	...	...
CANDELS J033203.24-274518.8 <sup>†</sup>	53.013517	-27.752123	3.2171	...	24.10±0.03 <sup>3</sup>	24.61±0.05 <sup>1</sup>	20.08±0.08 <sup>1</sup>	...	...	...	...
EIS U21 <sup>†</sup>	53.020574	-27.742151	3.4739	...	23.21±0.01 <sup>3</sup>	22.61±0.01 <sup>1</sup>	18.46±0.02 <sup>1</sup>	...	...	...	...
COMBO-17 352728	53.033345	-27.782362	2.6123	31.93±0.04 <sup>5</sup>	23.46±0.02 <sup>3</sup>	21.53±0.01 <sup>1</sup>	18.46±0.02 <sup>1</sup>	...	...	...	...
LQAC J03-027 007 <sup>†</sup>	53.034447	-27.698209	2.47	35.08±0.22 <sup>4</sup>	24.02±0.02 <sup>3</sup>	22.54±0.01 <sup>1</sup>	20.60±0.21 <sup>1</sup>	...	...	...	...
WISEA J033209.44-274807.3	53.039367	-27.801888	2.81	31.62±0.03 <sup>5</sup>	19.75±0.00 <sup>1</sup>	17.91±0.00 <sup>3</sup>	16.57±0.00 <sup>1</sup>	...	...	...	...
CANDELS J033217.41-274439.9	53.072567	-27.744446	2.6503	...	24.74±0.03 <sup>1</sup>	...	...	...	...	...	...
LQAC J03-027 027 <sup>†</sup>	53.078474	-27.850865	3.6609	33.64±0.09 <sup>5</sup>	24.53±0.02 <sup>1</sup>	21.16±0.00 <sup>1</sup>	18.90±0.05 <sup>1</sup>	...	...	...	14.69±0.25 <sup>2</sup>
CANDELS J033219.80-274518.9	53.08252	-27.755248	2.926	33.16±0.08 <sup>5</sup>	24.03±0.09 <sup>3</sup>	22.11±0.01 <sup>1</sup>	19.56±0.04 <sup>1</sup>	...	...	...	...
CANDELS J033222.17-274936.5	53.092455	-27.826868	2.54	36.49±0.27 <sup>4</sup>	25.02±0.04 <sup>1</sup>	21.01±0.00 <sup>1</sup>	19.52±0.07 <sup>1</sup>	...	...	...	19.74±0.15 <sup>3</sup>
CANDELS J033222.44-274543.8	53.093546	-27.762193	2.2807	34.26±0.16 <sup>4</sup>	24.45±0.01 <sup>1</sup>	19.28±0.06 <sup>1</sup>	19.55±0.12 <sup>1</sup>	...	...	...	...
CANDELS J033222.53-274804.3	53.093908	-27.801189	2.4117	35.33±0.10 <sup>4</sup>	24.04±0.04 <sup>3</sup>	22.63±0.10 <sup>1</sup>	19.55±0.12 <sup>1</sup>	...	...	...	...
GMASS 2443	53.100804	-27.715958	2.2979	33.97±0.10 <sup>4</sup>	22.43±0.01 <sup>3</sup>	21.33±0.00 <sup>1</sup>	19.62±0.05 <sup>1</sup>	...	...	...	...
CANDELS J033225.81-275120.4	53.107413	-27.855551	2.8779	35.26±0.14 <sup>4</sup>	24.19±0.05 <sup>3</sup>	22.41±0.01 <sup>1</sup>	20.91±0.15 <sup>1</sup>	...	...	...	...
CANDELS J033225.94-274514.3	53.108108	-27.753984	2.7228	33.28±0.06 <sup>5</sup>	23.71±0.02 <sup>3</sup>	22.15±0.01 <sup>1</sup>	20.99±0.46 <sup>1</sup>	...	...	...	...
CANDELS J033226.77-274603.9 <sup>†</sup>	53.111576	-27.767792	3.3313	34.26±0.09 <sup>2</sup>	26.44±0.04 <sup>3</sup>	22.28±0.01 <sup>1</sup>	20.54±0.20 <sup>1</sup>	...	...	...	...
CANDELS J033228.27-274403.4	53.117881	-27.73433	3.256	35.70±0.15 <sup>4</sup>	22.11±0.03 <sup>3</sup>	20.97±0.00 <sup>1</sup>	20.02±0.14 <sup>1</sup>	...	...	...	...
CANDELS J033228.77-274434.9	53.119858	-27.743092	3.0804	36.48±0.25 <sup>4</sup>	25.22±0.11 <sup>3</sup>	21.43±0.01 <sup>2</sup>	19.62±0.05 <sup>1</sup>	...	...	...	...
LQAC J03-027 039 <sup>†</sup>	53.124379	-27.851638	3.7098	32.70±0.06 <sup>5</sup>	23.53±0.02 <sup>3</sup>	21.28±0.00 <sup>1</sup>	18.81±0.02 <sup>1</sup>	15.71±0.67 <sup>1</sup>	...	...	15.65±1.41 <sup>2</sup>
CANDELS J033232.16-274651.4	53.134022	-27.780974	2.542	33.58±0.08 <sup>5</sup>	24.31±0.02 <sup>3</sup>	22.06±0.01 <sup>1</sup>	19.47±0.04 <sup>1</sup>	...	...	...	...
GMASS 2578	53.137581	-27.700116	2.4481	...	22.66±0.01 <sup>3</sup>	20.87±0.00 <sup>1</sup>	18.82±0.04 <sup>1</sup>	...	...	...	...
CANDELS J033233.24-274916.0	53.13851	-27.821132	3.4836	37.22±0.25 <sup>4</sup>	26.00±0.02 <sup>1</sup>	23.89±0.02 <sup>1</sup>	20.97±0.00 <sup>1</sup>	20.02±0.14 <sup>1</sup>	...	...	...
GMASS 2562	53.138699	-27.700492	2.4495	...	23.01±0.02 <sup>3</sup>	20.82±0.00 <sup>1</sup>	19.78±0.10 <sup>1</sup>	...	...	...	...
LQAC J03-027 045	53.148832	-27.821104	2.576	34.63±0.12 <sup>2</sup>	22.22±0.01 <sup>3</sup>	20.97±0.00 <sup>1</sup>	17.16±0.01 <sup>1</sup>	...	...	...	19.65±0.14 <sup>3</sup>
GOODS-CDFSS-MUSIC 15985	53.157456	-27.709059	2.9768	...	23.31±0.02 <sup>3</sup>	22.97±0.01 <sup>1</sup>	18.01±0.01 <sup>1</sup>	18.01±0.01 <sup>1</sup>	...	...	...
CANDELS J033238.15-274626.7	53.159	-27.774097	3.7148	...	28.57±0.05 <sup>1</sup>	...	...	...	...	...	...
GALEX-ASC J033238.92-274628.5	53.162258	-27.774725	2.447	...	20.55±0.00 <sup>1</sup>	20.77±0.00 <sup>1</sup>	18.90±0.03 <sup>1</sup>	...	...	...	...
GMASS 2467	53.162299	-27.712123	4.3792	34.41±0.19 <sup>2</sup>	24.04±0.01 <sup>3</sup>	20.72±0.01 <sup>1</sup>	19.19±0.04 <sup>1</sup>	...	...	...	...
GMASS 0253	53.163219	-27.808983	4.8759	35.10±0.19 <sup>2</sup>	23.91±0.00 <sup>4</sup>	22.20±0.01 <sup>1</sup>	22.68±0.16 <sup>1</sup>	...	...	...	...
GMASS 2043	53.174458	-27.733302	2.576	32.82±0.06 <sup>5</sup>	23.82±0.02 <sup>3</sup>	22.28±0.01 <sup>1</sup>	21.06±0.51 <sup>1</sup>	...	...	...	...
CANDELS J033242.83-274702.5	53.178486	-27.784035	3.166	32.61±0.05 <sup>5</sup>	23.80±0.00 <sup>2</sup>	23.09±0.01 <sup>1</sup>	13.62±0.32 <sup>1</sup>	...	...	...	...
HJD-JD	53.178696	-27.802639	2.4245	33.28±0.28 <sup>1</sup>	19.75±0.02 <sup>4</sup>	21.80±0.01 <sup>2</sup>	19.88±0.05 <sup>1</sup>	...	...	...	...
IRAC J03244.00-274635.0	53.183359	-27.776339	2.688	23.33±0.00 <sup>3</sup>	21.15±0.00 <sup>2</sup>	18.38±0.01 <sup>1</sup>	18.73±0.04 <sup>1</sup>	13.81±0.11 <sup>2</sup>	15.53±0.42 <sup>1</sup>	20.36±0.13 <sup>3</sup>	
SDSS J112355.73+621024.4	188.900099	62.173431	3.075	33.52±0.04 <sup>4</sup>	22.03±0.00 <sup>1</sup>	21.38±0.01 <sup>1</sup>	21.50±0.01 <sup>1</sup>	18.32±0.03 <sup>1</sup>	14.08±0.18 <sup>2</sup>	16.09±0.48 <sup>1</sup>	
LQAC 189+062 004 <sup>†</sup>	189.027919	62.264065	2.4135	32.94±0.04 <sup>4</sup>	22.80±0.01 <sup>1</sup>	21.50±0.01 <sup>1</sup>	18.22±0.06 <sup>1</sup>	14.03±0.33 <sup>3</sup>	16.00±0.35 <sup>1</sup>	21.48±0.30 <sup>3</sup>	
S-CANDELS J123611.92+621147.6	189.049878	62.196518	2.403	...	22.76±0.02 <sup>2</sup>	19.80±0.01 <sup>1</sup>	17.22±0.01 <sup>1</sup>	16.17±1.72 <sup>2</sup>	14.58±0.22 <sup>2</sup>	14.92±0.08 <sup>2</sup>	
WISEA J123623.00+621526.8 <sup>†</sup>	189.095583	62.253609	3.6539	35.08±0.04 <sup>8</sup>	22.75±0.00 <sup>1</sup>	22.04±0.00 <sup>1</sup>	19.39±0.05 <sup>1</sup>	18.81±0.11 <sup>1</sup>	15.50±0.18 <sup>2</sup>	18.09±0.15 <sup>3</sup>	
LQAC 189+062 014 <sup>†</sup>	189.139593	62.212858	3.413	33.93±0.04 <sup>6</sup>	25.01±0.03 <sup>1</sup>	22.67±0.00 <sup>1</sup>	20.69±0.28 <sup>1</sup>	...	...	...	23.01±1.18 <sup>3</sup>
S-CANDELS J123714.30+621751.1	189.186232	62.258635	2.453	...	24.44±0.02 <sup>1</sup>	22.95±0.01 <sup>1</sup>	20.41±0.16 <sup>1</sup>	...	...	...	16.86±1.50 <sup>2</sup>
S-CANDELS J123655.82+621201.1	189.218479	62.297495	3.905	...	24.92±0.02 <sup>1</sup>	24.01±0.02 <sup>1</sup>	19.52±0.08 <sup>1</sup>	18.08±0.01 <sup>1</sup>	13.92±0.19 <sup>2</sup>	14.92±0.08 <sup>2</sup>	
LQAC 189+062 059	189.27002	62.200212	2.737	35.28±0.04 <sup>7</sup>	22.71±0.02 <sup>1</sup>	20.86±0.01 <sup>1</sup>	18.81±0.11 <sup>1</sup>	...	...	...	...
S-CANDELS J123706.20+621844.2	189.275646	62.312224	2.414	...	24.56±0.06 <sup>1</sup>	20.93±0.15 <sup>3</sup>	18.81±0.11 <sup>1</sup>	...	...	...	20.21±0.19 <sup>3</sup>
S-CANDELS J123714.30+621808.5 <sup>†</sup>	189.30519	62.20236	3.1569	34.15±0.04 <sup>6</sup>	22.29±0.00 <sup>1</sup>	20.71±0.01 <sup>1</sup>	18.05±0.02 <sup>1</sup>	18.82±0.04 <sup>1</sup>	16.26±0.66 <sup>1</sup>	...	22.12±0.53 <sup>3</sup>
S-CANDELS J123719.43+621113.9	189.3309	62.187193	2.457	...	22.93±0.01 <sup>1</sup>	21.56±0.00 <sup>1</sup>	18.82±0.01 <sup>1</sup>	18.95±0.00 <sup>2</sup>	14.78±0.49 <sup>2</sup>	14.78±0.49 <sup>2</sup>	
LQAC 189+062 052	189.332675	62.165328	2.647	32.67±0.04 <sup>6</sup>	...	...	...	...	...	...	21.86±0.41 <sup>3</sup>

**Table 3** continued

**Table 3** (*continued*)

ID	RA (1)	Dec (2)	$z$ (3)	X-ray (4)	IR (5)	MIR (6)	FIR (7)	SMM (8)	Microwave (9)	Radio (10)	Radio (11)
S-CANDELS J123733.78+621345.2 <sup>†</sup> SDSS J123757.29+621627.3	189.390877 189.488797	62.22909 62.274298	2.386 31.75±0.04 <sup>4</sup>	22.24±0.01 <sup>1</sup> 21.61±0.00 <sup>1</sup>	20.73±0.00 <sup>1</sup> 20.42±0.00 <sup>1</sup>	18.03±0.01 <sup>1</sup> 18.37±0.03 <sup>1</sup>	15.64±1.71 <sup>2</sup> ...	...	22.17±0.56 <sup>3</sup> ...	22.36±0.74 <sup>3</sup>	

## NOTE—

Tabulated AB-magnitudes of the highest SNR band in the following spectral ranges:

X-ray: <sup>1</sup>Chandra 0.2–0.5 keV, <sup>2</sup>Chandra 0.5–10 keV, <sup>3</sup>Chandra 0.5–2 keV, <sup>4</sup>Chandra 0.5–7 keV, <sup>5</sup>Chandra 0.5–8 keV, <sup>6</sup>Chandra 2–8 keV, <sup>8</sup>Chandra 4–8 keVIR: <sup>1</sup>CFHT/WIRCam  $K$ , <sup>2</sup>HST/WFC3-IR F125W, <sup>3</sup>HST/WFC3-IR F160W, <sup>4</sup>HST/NICMOS F160W, <sup>5</sup>VLT/ISAAC  $K_s$ , <sup>6</sup>VISTA/VIRCAM  $J$ MIR: Spitzer/IRAC <sup>1</sup>3.6  $\mu$ m, <sup>2</sup>4.5  $\mu$ m, <sup>3</sup>5.8  $\mu$ mFIR: <sup>1</sup>Spitzer/MIPS 24  $\mu$ mSMM: <sup>1</sup>LABOCA 870  $\mu$ m, <sup>2</sup>SPIRE 250  $\mu$ m, <sup>3</sup>SPIRE 350  $\mu$ mMicrowave: <sup>1</sup>AzTEC 1.16 mmRadio: <sup>1</sup>ATCA/CABB, <sup>2</sup>VLA L-band.<sup>†</sup> indicates a LyC leaker.